Comparison of Mechanical Vapour Compression Evaporator Technologies

by

Victor McLafferty

Submitted in partial fulfilment of the requirements
for the degree of **Master of Applied Science**

at

Dalhousie University
Halifax, Nova Scotia
April 2018

Table of Contents

List of Tables

List of Figures

Abstract

The energy efficiency, heat exchanger area requirements, and solids handling performance of Mechanical Vapour Compression (MVC) evaporation were compared to a proposed evaporator configuration called Mechanical Vapour Compression Flash Distillation (MVC-FD). Steady-state models were developed for both systems, and their thermal performance was compared. It was found that the MVC-FD configuration significantly increases specific energy consumption and heat exchanger requirements when compared to the standard MVC configuration. A steady-state bulk fouling model was developed for $CaSO_4$-H_2O-NaCl to determine whether fouling is reduced using the MVC-FD configuration. It was found that fouling is increased in this system due to the solubility properties of $CaSO_4$. Fouling was also examined for the NaCl-H_2O fluid system. It was found that the fouling can be substantially reduced by the MVC-FD system because fouling in this system is driven primarily by liquid volume change.

List of Abbreviations and Symbols Used

Abbreviations

MED	Multiple-Effect Distillation
MSF	Multi-Stage Flash
MVC	Mechanical Vapour Compression
MVC-FD	Mechanical Vapour Compression Flash Distillation
RO	Reverse Osmosis
SEC	Specific Energy Consumption

Symbols

ΔH	Change in enthalpy (kJ/kg)
ΔT_H	Condensation – evaporation temperature difference (°C)
ΔT_{lm}	Log-mean temperature difference
ΔT_N	Change in temperature across flash nozzle (°C)
μ	Ionic strength (mol/kg)
B	Mass flow rate of concentrate (kg/s)
c_{Bo}	Specific heat capacity of exiting concentrate (J kg^{-1} $°C^{-1}$)
c_{co}	Specific heat capacity of liquid condensate (J kg^{-1} $°C^{-1}$)
c_f	Specific heat capacity of feed exiting preheater (J kg^{-1} $°C^{-1}$)
c_{pre}	Specific heat capacity of feed entering preheater (J kg^{-1} $°C^{-1}$)
c_{sw}	Specific heat capacity of seawater (J kg^{-1} $°C^{-1}$)
c_v	Specific heat capacity of seawater in separation vessel (J kg^{-1} $°C^{-1}$)
D	Dielectric constant
F_i	Mass flowrate of feed (kg/s)

H_c	Specific enthalpy of compressed vapour (kJ/kg)
H_{con}	Specific enthalpy of condensate (kJ/kg)
H_t	Specific enthalpy of vapour in separation vessel (kJ/kg)
K^o	Solubility product
L	Mass flow rate of recirculated feed (kg/s)
m	Molality (mol/kg of solvent)
P_c	Compressor outlet pressure (kPa)
P_t	Separation vessel pressure (kPa)
$p_{v,sw}$	Vapour pressure of seawater (kPa)
$p_{v,w}$	Vapour pressure of water (kPa)
Q_s	Change in enthalpy of condensing steam (J kg^{-1} s^{-1})
R_f	Mass flow rate exiting main heat exchanger (kg/s)
R_i	Mass flow rate exiting flash nozzle (kg/s)
S_p	Salt concentration (g/kg)
T_{con}	Condensation temperature (°C)
T_f	Temperature of feed exiting preheater (°C)
T_o	Temperature of exiting concentrate/distillate (°C)
T_{pre}	Feed temperature (°C)
T_s	Steam temperature at compressor outlet (°C)
T_t	Separation vessel liquid temperature (°C)
U_o	Overall heat transfer coefficient (W m^{-2} K^{-1})
V	Vapour flow rate (kg/s)
W	Compressor work (J/s)
x^*	Saturation concentration (g/kg)
x_i	Feed salt concentration (g/kg)

x_t	Separation vessel salt concentration (g/kg)
x_v	Concentrate salt concentration (g/kg)
γ	Activity coefficient
ε	Isentropic efficiency
ρ_w	Density of water (g/cm^3)
τ	Precipitation to reach saturation concentration (g/s)
ϕ	Recovery ratio (concentrate/feed)

Acknowledgements

I would like to thank Dr. Jan Haelssig for providing me the opportunity to work on this research. His guidance, patience, and support have been instrumental to the completion and success of this project.

I would also like to thank my committee members, Dr. Stephen Kuzak and Dr. Dominic Groulx, for reviewing my work and for their suggestions.

Additionally, I would like to thank my mother and father, and Taylor, who have provided endless amounts of support without which I could not have completed this work.

Chapter 1

Introduction

Freshwater is required for many important functions, from the maintenance of basic health to the requirements of modern industry. In recent times, significant concern regarding the future availability of water resources has arisen, as freshwater has become an overstressed natural resource. Water scarcity is currently impacting 700 million people. It is predicted that this amount will increase to 2.8 billion by 2025 (Hameeteman, 2013). This shortage of water will not only create human health problems such as dehydration and sanitation issues, but it will also lead to limitations on agricultural productivity and industrial development, reducing and inhibiting the quality of life of many people all around the world. Technology is needed to produce freshwater to eliminate water scarcity issues.

A wide range of technologies are being used to convert seawater to freshwater to meet regional water demand. The process of converting saltwater to freshwater is referred to as desalination. This is but one type of application where the process separates a solution into a variety of components. Technologies that accomplish such a task are typically referred to as separation technologies. In the case of desalination, seawater is separated into a concentrated brine and freshwater.

The separation technologies used for seawater desalination can be divided into thermal technologies and membrane technologies (Shatat et al., 2014). Although other systems have been proposed, most commercial membrane systems use reverse osmosis (RO). Conversely, thermal separation systems use different configurations of evaporators. These processes are very similar to those used for the separation of solvents from dissolved solutes in a wide range of other applications.

A simplified diagram of a reverse osmosis system being used to desalinate water is shown in Figure 1.1. Membrane separation technologies like RO characteristically use a semi-permeable barrier that allows passage of certain components of a solution and impedes others, allowing for the concentration of rejected components, or the purification of

permeated components. The process in Figure 1.1 shows seawater being pumped into a RO module. The seawater is placed under enough pressure to exceed the osmotic pressure of the seawater and thus promote flow across the semi-permeable membrane (Prante et al., 2014). The membrane inhibits flow of dissolved salts. This allows their removal from the permeate. As permeate is removed from incoming seawater the solute is concentrated leading to the formation of concentrated saline water (brine).

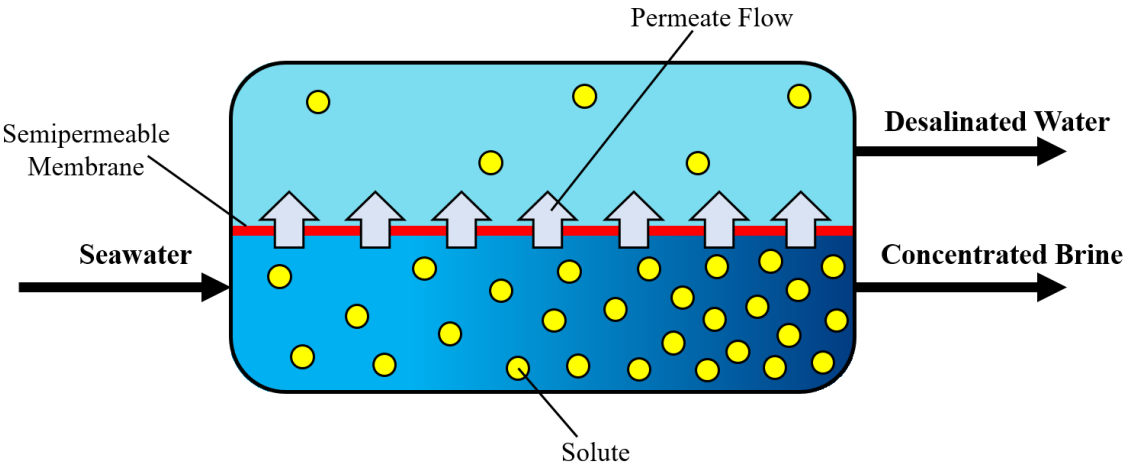

Figure 1.1: Simplified RO desalination flow diagram

Thermal separation technology relies on evaporation, phase change, and difference in vapour pressures of solution components to remove solvent from solutions. Thermal technologies can be as simple as a single-effect evaporator, as illustrated in Figure 1.2, for separating components with large differences in vapour pressures, such as is the case with applications where a liquid component is to be separated from a dissolved solid. Simple evaporators require significant energy costs due to the high energy associated with the latent heat of evaporation of a substance.

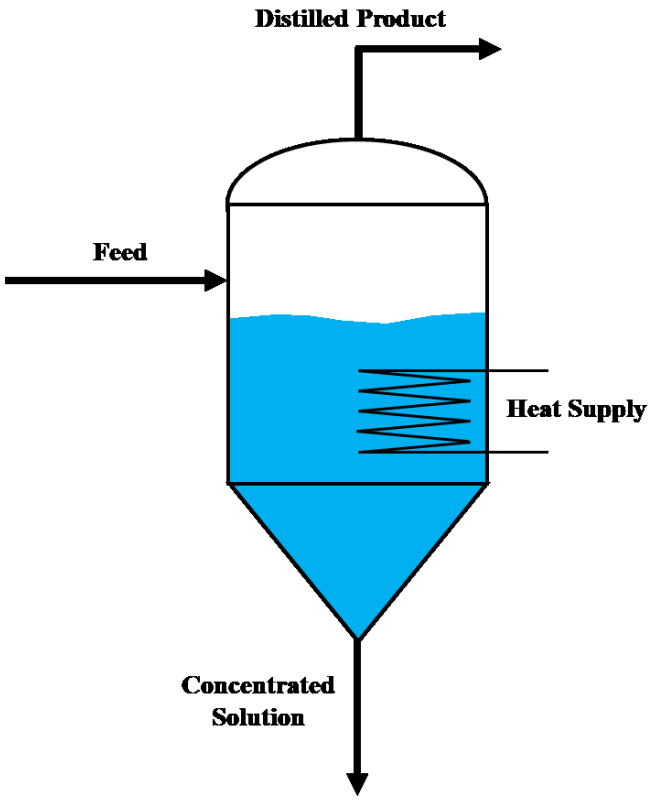

Figure 1.2: Single-effect evaporator

Many technologies have been developed to combat this high energy cost; one such technology is multi-stage flash distillation (MSF). MSF recovers latent heat by using a series of stages set at different pressures, in which the feed is heated by the condensing distillate product (Khawaji et al., 2008). A simplified process flow diagram for MSF is shown in Figure 1.3. The diagram shows three flash stages, though it is possible to use more for improved energy efficiency. Feed seawater enters the third stage, where it acts as cooling fluid to condense vapours coming from the brine. The seawater again acts as the cooling fluid in stages 1 and 2. Additional heating is provided to the feed seawater by steam heating. The heated seawater proceeds through stages 1 through 3. Each stage operates at a lower pressure than the previous, which allows flashing to occur. Flashed vapour provides partial heating to the feed seawater, recycling latent heat. Concentrated brine exits the final stage along with desalinated water. These types of systems require significant capital investment when compared to simple single-effect evaporators but are generally worth the capital expense due to their increased energy efficiency (Shatat et al., 2014).

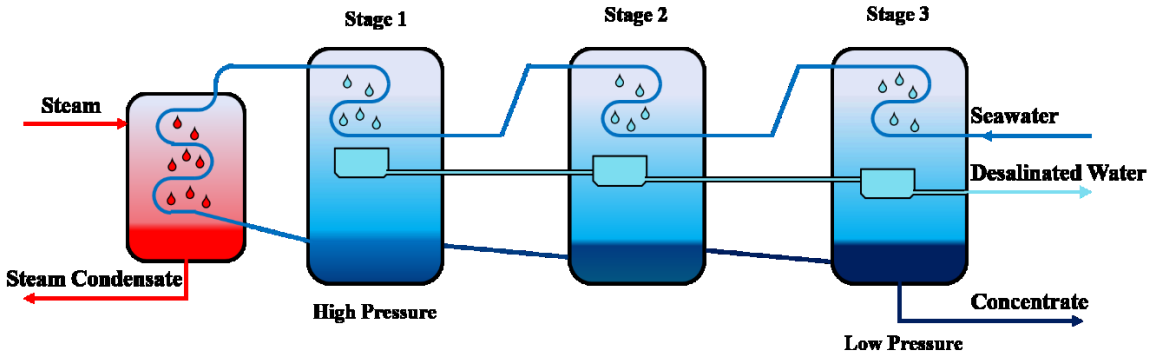

Figure 1.3: Multi-stage flash distillation

Other thermal technologies operate on the principle of recycling latent heat to improve energy performance. One such technology is mechanical vapour compression (MVC), which uses a mechanical compressor to increase the pressure and temperature of distillate vapour to use it as the heating fluid for the incoming seawater feed (Darwish, 1988). Figure 1.4 shows a simplified process diagram for an MVC desalination system.

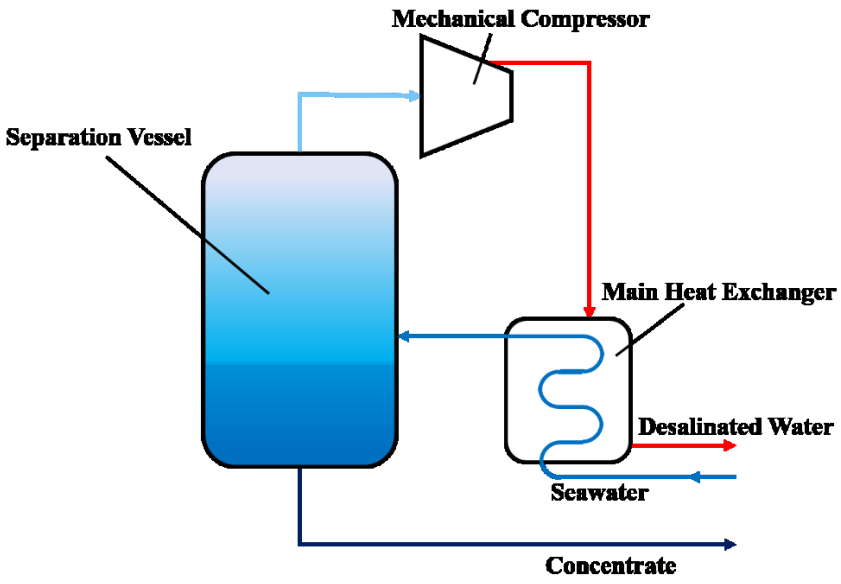

Figure 1.4: Mechanical vapour compression desalination process

Thermal separation technologies have long dominated in the petrochemical and bulk chemical production industries, though with recent developments in membrane technologies this is beginning to change. For example, the desalination industry which has

historically been dominated by thermal processes such as MSF now mainly uses reverse osmosis, a membrane technology (Koros, 2004). Sixty percent of installed desalination capacity comes from facilities using reverse osmosis (Manjula et al., 2013). The growing use of reverse osmosis in the desalination industry is driven by its low specific energy consumption (SEC) (kWh/m^3 produced freshwater) when compared to the competing thermal technologies (Fritzmann et al., 2007). The typical SEC of reverse osmosis and other thermal technologies when used for desalination are shown in Table 1 (Stillwell et al., 2016).

Table 1.1: Specific Energy Consumption of Desalination Technologies. Data from Stillwell et al. (2016).

Technology	Specific Energy Consumption Total Electric Equivalent (kWh/m^3)
Reverse osmosis (RO)	3-6
Multi-stage flash (MSF)	21-59
Multiple-effect distillation (MED)	15-57
Mechanical vapor compression (MVC)	7-15

Despite their significantly higher energy cost, thermal technologies still find widespread use in chemical separation applications due to their wide range of applicability. Moreover, the efficiency of membrane systems like RO are impacted by the solids content in the feed (Burn et al., 2015). Perhaps with the development of newer materials the applications of membrane technology will grow, but thermal technologies continue to dominate industry due to their wide versatility, ease of use, and the cost associated with replacing current infrastructure.

The technologies displayed alongside reverse osmosis in Table 1 (MSF, MED, and MVC) are all thermal separation technologies relying on evaporation to separate water from brine. Though most thermal technologies have much worse SEC than RO, the SEC of MVC technology is only marginally higher than RO, relative to the SEC requirements of the other thermal technologies, MED and MSF. MVC has a higher energy efficiency because the steam evaporated from solution gets compressed and is used to provide heat for incoming process fluid. The low specific energy consumption combined with the robustness of

thermal separations in response to different feed conditions (Fritzmann et al., 2007) make MVC evaporators useful in a wide range of applications.

Like other thermal separation technologies, MVC evaporators suffer from a significant maintenance issue known as scaling, i.e. the build up of solid precipitates on heat exchange surfaces. Scale inhibits heat transfer, reduces performance and increases specific energy requirements. Prevention and mitigation are the best ways of handling fouling problems because relying on maintenance can be costly and often requires significant process downtime. Supersaturation of a dissolved salt is the primary mechanism for its precipitation (Jamialahmadi et al., 2010). Supersaturation of a salt can occur for a variety of reasons. In evaporation operations, the change in liquid volume as fluid changes phase leads to an increase in the concentration of dissolved salts in the liquid phase above saturation concentrations (Wittering, 2015). In addition, the solubility of many salts is inversely proportional to temperature, such that large increases in temperature decrease the saturation concentration below the dissolved salt concentration, leading to precipitation (Jamialahmadi et al., 2010).

Preventing liquid volume change may reduce fouling in heat exchanging equipment. With this concept in mind, a modification was proposed for MVC evaporator systems. The following section discusses an alternative to MVC evaporation that improves capacity for solids handling while maintaining high thermodynamic efficiency.

1.1 MVC and MVC-FD Outline

This section covers the basic configuration of two different mechanical vapor compression systems. The first configuration is presented as the standard set-up for most MVC systems. The second configuration is presented as an alternative to standard MVC and is called mechanical vapour compression flash distillation (MVC-FD). The MVC-FD system is proposed as an option that will produce less scaling on heat exchange surfaces than the standard MVC desalination systems by preventing evaporation in heat exchangers.

Figure 1.5 shows the flow diagram for a typical MVC desalination system. The system shown includes a preheater, separation vessel, compressor, feed pump, and main heat exchanger. Items such as pre-treatment equipment, filters, auxiliary pumps, de-

superheating equipment, and auxiliary heaters have been excluded. Key components are numbered in red. The system operates by pumping seawater contained in the feed tank (1) through the preheater (2). The preheater heats the feed using energy recovered from high-temperature distillate (6) and concentrate (7) streams. After passing through the preheater, the feed is then pumped through the main heat exchanger (3). The feed is partially evaporated so that it forms a two-phase mixture of water vapour and concentrated seawater. Energy for evaporation of the feed in the main heat exchanger is provided by condensing steam arriving from the compressor (5). The pressure on the feed side is lower than on the steam side so that the steam from the compressor may condense at a higher temperature than the boiling temperature of the feed, thus allowing heat exchange to occur across the heat exchanger. The two-phase mixture enters the separation vessel (4), where liquid and vapour components of the feed stream can separate. Concentrated seawater, termed concentrate, flows back to the preheater (2) to allow for heat recovery. Water vapour in the separation vessel (4) is drawn into the compressor (5) where its pressure and temperature increase through mechanical work. The compressed stream is then passed to the main heat exchanger for condensation. The condensate produced is passed through the preheater to recover any remaining heat and exits the system as freshwater (7).

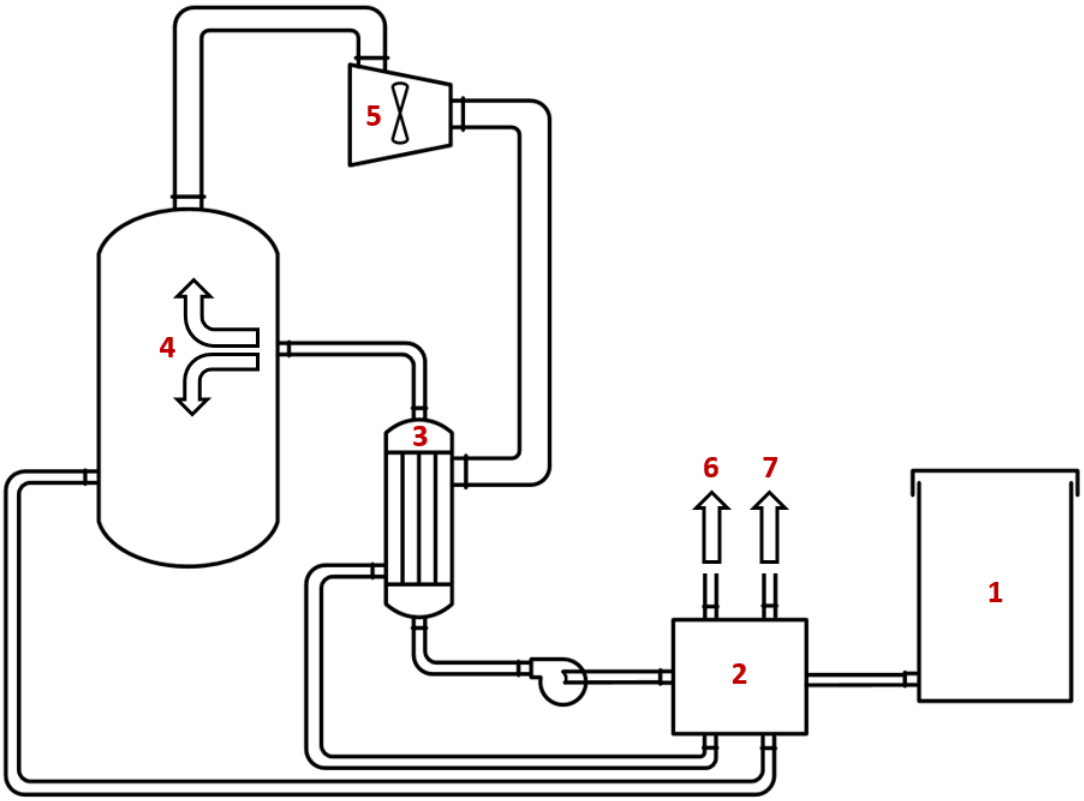

Figure 1.5: Standard MVC evaporator system

In some systems, a recirculation loop is added to increase the velocity of the tube-side liquid in the main heat exchanger to increase heat transfer rates. The two variations of this are forced circulation systems, which use a pump to set the recirculation flow rate, and thermosiphon systems, which use the change in liquid density due to heating as a driving force for recirculation. Forced circulation systems are more common in applications if the process fluid is highly viscous.

Scale formation may occur on heat transfer surfaces in all types of thermal desalination processes. Scale formation inhibits heat transfer, which leads to increased system specific energy consumption and costly maintenance requirements (Krömer et al., 2015). Scale is formed by the precipitation of salts from solution. Based on feed conditions, such as temperature and pH (Rahman, 2013), there exists a maximum concentration of salt that can exist in solution. Introducing additional salt or removing solvent so that the concentration exceeds this maximum concentration will lead to the precipitation of salt and the formation

of scale. This parameter is typically referred to as the solubility limit, or saturation concentration. Evaporation of seawater has the potential to concentrate dissolved salts past their solubility limits, thereby causing solids precipitation and scale formation. When evaporation of the feed occurs in the heat exchanger of the MVC desalination system, a potential for fouling exists. Limiting recovery (low distillate production) is a viable way to reduce solids precipitation due to change in fluid volume; however, there are many reasons that make operating at a high distillate recovery desirable. High distillate recovery allows for lower feed intakes, while also reducing the amount of brine that is discharged. This reduces the environmental impact of the process, and in circumstances where waste streams cannot be released to the environment, it also minimizes the amount of waste handling. Additionally, economic factors encourage high distillate recovery. Operating at high distillate recovery gives a higher rate of distillate production per capital amount invested.

Figure 1.6 presents an alternative MVC desalination configuration that aims to reduce evaporation in the heat exchanger to reduce scale formation while maintaining a high recovery of distillate (MVC-FD). The differences between the standard MVC configuration presented and MVC-FD are shown in Figure 1.6 and include a recirculation loop (8) and a flash nozzle (9). The flash nozzle is added to pressurize the feed on the tube side of the main heat exchanger to prevent evaporation. Once feed passes through the nozzle, it will spontaneously evaporate (i.e. flash) due to the decreased pressure in the separation vessel. This moves precipitated solids into the separation vessel, where they can be collected by some solids handling device such as a filter or a cyclone. The recirculation loop (8) is included to allow more control over the proportion of feed flashed. This is explained in detail in subsequent sections.

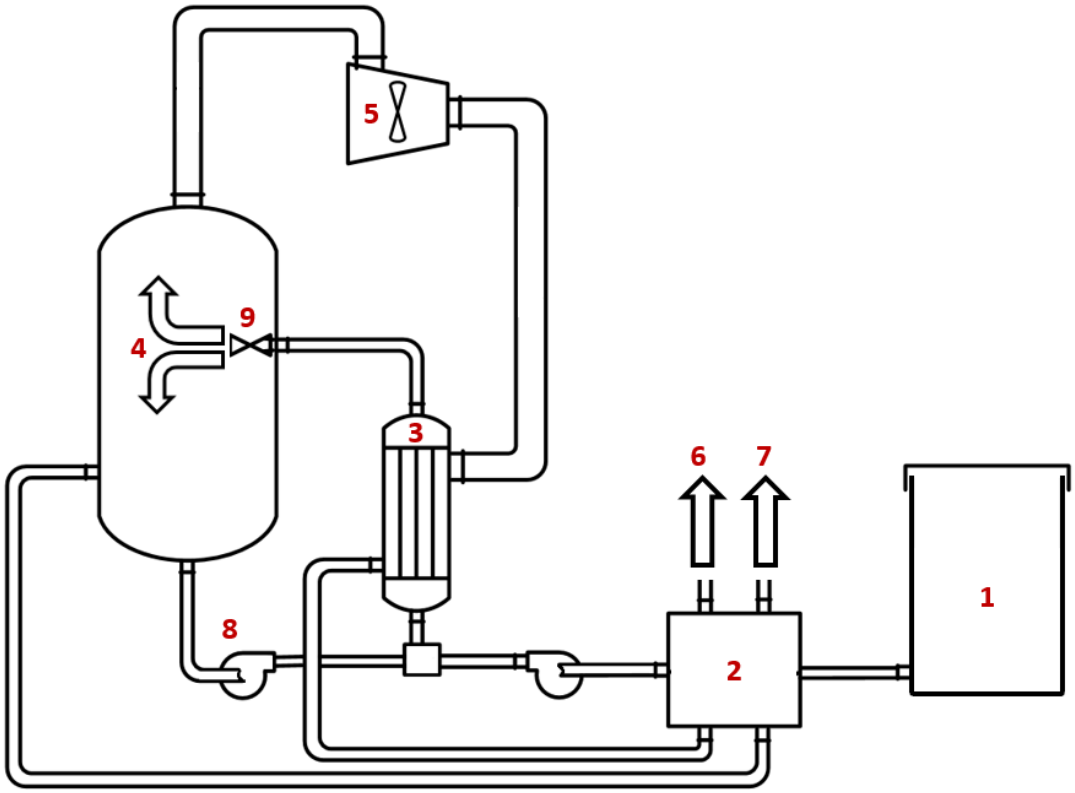

Figure 1.6: MVC-FD evaporator flow diagram

MVC evaporators use steam compression to recycle latent heat and reduce energy requirements, making them more efficient than other thermal separation processes. The MVC-FD system maintains this key heat recycling component while adding a flash nozzle, the purpose of which is to prevent evaporation on heat exchange surfaces and thereby reduce fouling. The hypothesis is that this change will reduce scaling while only marginally increasing energy requirements. The two systems were compared in this study using the models developed to substantiate this hypothesis.

The objective of this work is to compare MVC evaporator systems to a proposed alternative, Mechanical Vapour Compression Flash Distillation (MVC-FD). A steady-state model was made to compare the energy efficiency and equipment requirements of the two systems. The potential of the MVC-FD to reduce scale formation was evaluated by developing a fouling model to calculate the maximum fouling rates of the two systems.

Chapter 2

Background

This section discusses some of the work and the conclusions that some researchers have reached regarding the application of MVC systems and their thermodynamic performance, as well as scaling in thermally-driven systems.

2.1 MVC Evaporators

Darwish (1988) performed thermal analysis and heat exchanger sizing on a MVC evaporator system applied to the desalination of water. The heat exchanger sizing was done for a horizontal tube evaporator (HTE) for a correlation deduced from work by Takada et al. (1983). The application of this correlation is not valid for MVC-FD configurations. Steady-state modelling is used as the basis of the analysis by Darwish (1998). Included in this work is an analysis showing increased performance of MSF desalination systems when combined with vapour compression. Darwish suggests that RO and MVC systems are quite competitive in desalination applications, especially where there is a significant risk of fouling. The work provides steady-state models for calculating performance, though fluid properties like heat capacity are assumed to be constant to simplify the model. Ettouney (2006) provides a similar thermodynamic analysis of an MVC desalination system as well as design calculations for specific related equipment such as those for evaporator sizing, demister specifications, and system venting capacity. Similar thermodynamic studies for MVC applied to desalination have also been done by Aybar (2002). Modeling work by Ettouney (2006), Darwish (1998), and Aybar (2002) assume heat losses from the equipment to the environment are negligible. Ettouney (2006) suggests that for an actual MVC system design the heat exchanger area would be 2 to 5% greater than predicted through modeling because of the assumption that heat losses are negligible. Additionally, most MVC modelling work assumes that dissolved solids do not carry over into the distilled product, such as in the work by Ettouney (2006).

Bahar et al. (2004) performed and examined studies on a two-effect MVC desalination system and determined the effect of brine concentration and compressor speed on an

operational parameter they define as the "performance ratio". They determined that increasing compressor speed improved this parameter. This parameter is analogous to SEC, which can be calculated from their raw data. From their raw data, it is calculated that the SEC of their system is between 26.2 and 74.5 kWh/m^3. The SEC decreases with increasing compressor speed. Although this range of SEC values shows a significant deviation from the values of 7 to 15 kWh/m^3 reported by Stillwell et al. (2016), it should be noted that they were limited by compressor capacity and could not increase compressor speed past 2400 rpm. If they had used a more capable compressor, it is likely that lower SEC values would have been achieved.

Veza (1995) reviewed performance data for two MVC desalination units and reported that the SEC of the units ranged from 10.4 to 11.2 kWh/m^3, indicating a much better performance than that shown by Bahar et al. (2004). This reinforces the suggestion that the high SEC values shown by Bahar et al. were the result of compressor limitations. The range determined by Veza (1995) also verifies the upper portion of the range of SEC achievable reported by Stillwell et al. (2016), as the range reported by Veza (1995) is within 7 to 15 kWh/m^3.

Much of the analysis of MVC evaporators is focused on their application in desalination, though they can also be used in other applications to improve energy performance. This is shown by some of the modelling and experimental work for MVC systems that has been done for applications outside of desalination. This is the case with the work by Zhou (2014), where modelling was done to determine heat exchanger sizing and energy requirements for an MVC evaporator system processing wastewater containing Na_2SO_4. An experimental system was built, and a comparison was made between the experimental results and those from the model. It was shown that the model by Zhou et al. (2014) significantly underpredicted SEC. Work by Sandei et al. (2003) showed the versatility of MVC evaporators by examining experimental results of an MVC evaporator used to concentrate a variety of food products including apple juice, rectified grape must, tomato juice, orange juice, and dealcoholized yeast.

MVC can also be applied to separations where the two solution components to be separated have close boiling points. This is shown in the work by Oliveira et al. (2001) where thermodynamic modelling illustrated that the incorporation of vapour compression into an enthanol-water distillation column can reduce the specific energy consumption of the system. Patents have been filed that seem to indicate MVCs' usefulness in other applications. For example, U.S. Patent US6120651 (Gammon et al., 1998) describes a system that can be used for removing water from an aqueous fluid mixture, specifically a mix of ethylene glycol and water. This system is of note due to the large difference in boiling points between ethylene glycol (197.1°C at 1 atm) (MEGlobal, 2008) and water (100°C at 1 atm). The major components of the system include a vapour compression system to recycle steam in the manner of an MVC evaporator.

In published work, few references are made to MVC systems that use flashing to avoid scaling of heat exchanger surfaces. European patent EP1798202B1 (Kishi, 2004) refers to a system in which the heat exchanger is pressurized to prevent boiling in heat exchanging equipment; however, it does this by using liquid head instead of a pump and a nozzle, which can be used to achieve the same effect. The system as outlined would not likely achieve its goals because the height of liquid needed to achieve a pressure high enough to prevent boiling would need to be quite significant. No other literature could be found that outlines steady-state modelling or performance predictions of the proposed MVC-FD system.

2.2 Scale Formation

The general types of heat exchanger fouling processes are described in the work by Awad (2011). He divided them as follows: particulate fouling, precipitation fouling, chemical reaction fouling, corrosion fouling, biological fouling, and solidification fouling. For systems heating and processing seawater or liquids containing dissolved solids, precipitation fouling is common (Awad, 2011). This suggestion is echoed by Stark et al. (2017) who suggested that precipitation fouling is a "severe" problem in MED plants processing seawater. The undesirable precipitation fouling functions on principles similar to those of crystallization processes, in which supersaturation drives crystal formation (Kind, 1990). Precipitation can thus occur when the concentration of the dissolved

component in a solution surpasses its saturation concentration and becomes supersaturated. If the concentration of the dissolved component is below its saturation concentration, it is said to be stable (Wittering, 2015), and precipitation does not occur. A supersaturated solution can be classified based on its degree of supersaturation as either metastable, or labile (Wittering, 2015). In both labile and metastable states crystallization will occur with the presence of previously formed crystals, though in the labile state crystals will also spontaneously nucleate (Wittering, 2015). Changes in temperature often impact the solubility curve of a dissolved compound in solution (Mota et al., 2009), but other factors can play a role in solubility, such as the concentration of additional dissolved components. This is shown for the NaCl-$CaSO_4$-H_2O system by the solubility data collected by Power et al. (1966), where the concentration of dissolved NaCl impacts the solubility of $CaSO_4$. A hypothetical solubility curve for a solid indicating the labile, metastable, and stable regions is shown in Figure 2.1, where x^* is the saturation concentration for a given temperature, T.

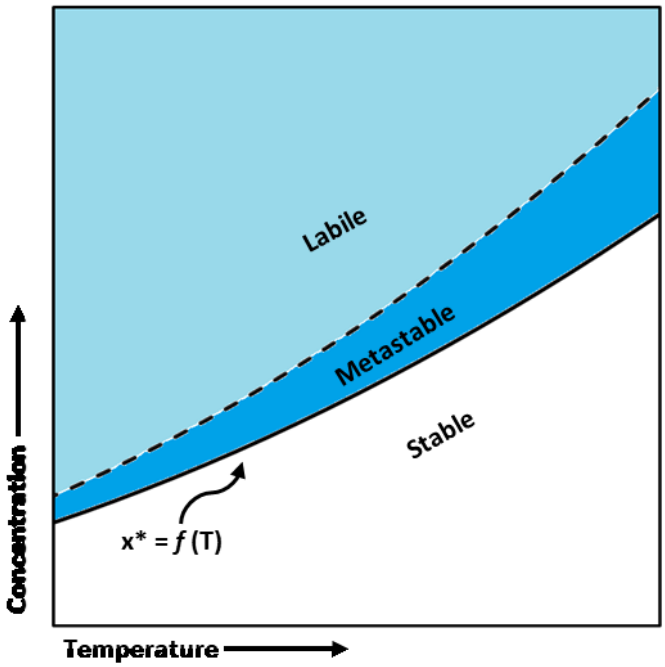

Figure 2.1: Solubility diagram for a solid in which solubility increases with temperature.

For systems in which solubility increases with temperature, supersaturation can be reached without adding solid by either reducing the temperature such that the saturation concentration decreases lower than the current solution concentration, or via evaporation whereby dissolved solids are concentrated past solubility limits by liquid volume change (Wittering, 2015). Some solid-liquid systems have inverse relationships with temperature and solubility concentration like that of $CaCO_3$-H_2O (Jamialahmadi, 2010). In such cases, temperature increases can lead to the solution becoming supersaturated. The process of precipitation resulting from evaporation, and heating, is shown for a solid-liquid system with an inverse temperature-solubility relationship in Figure 2.2. The degree of supersaturation resulting from either concentration or solubility changes from heating is defined in equation 1 (Kind, 1990):

$$\Delta x = x - x^* \tag{1}$$

where x is the concentration of the dissolved component, and x^* is the saturation concentration. The greater the degree of supersaturation resulting from temperature changes or evaporation, the greater the driving force for precipitation, and the more rapidly precipitation will occur (Kind, 1990).

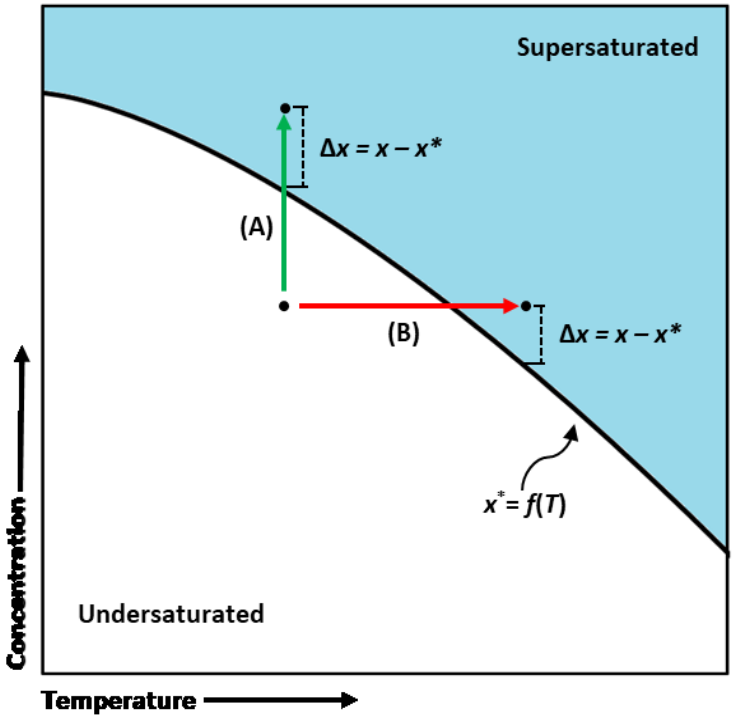

Figure 2.2: Solubility diagram for inversely soluble solid-liquid system. Precipitation can occur through either (A) evaporation at constant temperature or (B) heating.

Developing a model for an MVC system applied to desalination requires the use of property correlations for seawater, as well as an understanding of its composition. Sharqawy et al. (2009) provide a comprehensive review of seawater property correlations reported in literature. Correlations to calculate properties such as specific heat capacity, and boiling point elevation are provided in this work (Sharqawy et al., 2009). The application of these correlations to the steady-state MVC and MVC-FD models is discussed further in section 3.4. For modelling, feed conditions need to be specified. Typically, seawater salinities are at approximately 35 g/kg (Krömer et al., 2015). The salinity of seawater is a result of many contributing dissolved ions. The work by Kester et al. (1967) provides tabulated data for typical ionic composition of seawater. This data is shown in Table 2.1.

Table 2.1: Ionic Composition of Dissolved Components of Natural Seawater. From Kester et al. (1967)

Ion	Concentration (g/kg)
Cl^-	19.353
Na^+	10.76
SO_4^{2-}	2.712
Mg^{2+}	1.294
Ca^{2+}	0.413
K^+	0.387
HCO_3^-	0.142
Br^-	0.067
Sr^{2+}	0.008
H_3BO_3	0.026
F^-	0.001
Total	**35.163**

According to Table 2.1, the major ionic constituents of seawater are Cl^- and Na^+. Together they account for 85.6% of the salinity of seawater; however, despite their high concentration, it is the other constituents that are typically responsible for fouling in heat exchange equipment processing seawater. The literature indicates that for seawater evaporation fouling in heat exchange equipment primarily takes the form of calcium or magnesium compounds (Krömer et al., 2015). More specifically, calcium carbonate ($CaCO_3$), magnesium hydroxide ($Mg(OH_2)$), and calcium sulfate ($CaSO_4$) are the primary components of fouling precipitates and scale (Alsadaie et al., 2017). Some researchers have suggested that calcium sulfate fouling can be prevented entirely by avoiding operating temperatures under 120°C (Alsadaie et al., 2017; Al-Sofi, 1999). However, Krömer et al. (2015) have demonstrated that this is not true through the examination of scaling on heat exchange surfaces used for desalination of various synthetic seawater compositions under different temperatures (Krömer et al., 2015). One of the experiments conducted by Krömer et al. (2015) demonstrated that for elevated seawater compositions, and evaporation at a temperature of 75°C, scaling was largely composed of $CaCO_3$ in the form of aragonite, with a base layer composed of magnesium-based crystals. $CaSO_4$ was also detected, interspersed between $CaCO_3$ crystals. This indicates that $CaSO_4$ begins to form at much

lower temperatures than indicated in other work (Alsadaie et al., 2017; Al-Sofi, 1999). However, there is agreement that at low temperatures $CaSO_4$ formation is inhibited when evaporation occurs at lower temperatures. In the work of Krömer et al. (2015), no formation of $CaSO_4$ was indicated at low temperature evaporation and scale was primarily composed of calcium carbonate. In either case, calcium carbonate-based compounds are the main source of scaling during seawater evaporation (Krömer et al., 2015).

Solubility data is crucial to determine whether precipitation of a dissolved component from solution will occur (Rahman, 2009). The saturation concentration of a dissolved component is a measurement that indicates the maximum amount of a component that can exist dissolved in solution. Solutions with concentrations greater than the saturation concentration (i.e. supersaturated) will tend to form precipitate (Rahman, 2009). Seidell (1919) presented a comprehensive review of solubility data for a large range of inorganic and organic compounds. The solubility data for a NaCl-H_2O system is of interest because it is used in subsequent sections of this work. Power et al. (1966) measured solubility data for $CaSO_4$-NaCl-H_2O systems, and used their solubility data to develop a model capable of predicting the saturation concentration of $CaSO_4$ in H_2O-NaCl solution for various temperatures and salinities based on calculated solubility products from the collected solubility data, and the theory of thermodynamic properties of electrolytic solutions (Power et al., 1966). This is clarified further in section 4.1. The solubility data from Power et al. was shown to agree with data from other works.

Esawy et al. (2017) performed experimental work and proposed a model for $CaSO_4$ crystallization fouling in finned tubes for a nucleate boiling regime. The model incorporates the kinetics of the deposition process, as well as numerous other variables such as bubble size, and microlayer concentration, fluid velocity, and solids removal rate to predict the evolution of fouling resistance to heat transfer over time (Esawy et al., 2017). Models that require variables such as fluid velocity require specific equipment selection and sizing to be calculated. As such, application of detailed models such as that by Esawy et al. (2017) have strict limitations.

Chapter 3

Modelling of Mechanical Vapour Compression Evaporators

To justify the development of Mechanical Vapour Compression Flash Distillation (MVC-FD) as a worthwhile technology to investigate further, a comparison must be made between it and the standard Mechanical Vapour Compression (MVC) configuration. This study aims to examine the potential of MVC-FD by presenting the difference in energy consumption and equipment sizing between it and the standard MVC configuration.

Comparison of the two systems was made from the results of mathematical modelling at steady-state, with the objective of obtaining operational ranges and limitations, comparing energy efficiency, and performing basic equipment sizing. A few assumptions were applied to both models for simplification purposes:

- No heat loss to the environment
- Feed pumping requirements are considered small relative to other requirements
- Perfect phase separation in the separation vessel

A few other assumptions are applied, but these are specific to each system model, and are discussed in each system's respective modelling description.

3.1 Steady State Modelling Overview

Mechanical vapour compression (MVC) is a technology that uses the compression of steam generated through evaporation of a liquid to supply heat for the evaporation, creating a "self-heating" process and essentially recycling a significant portion of the heat associated with evaporation. The pressurized vapour will condense at a higher temperature than the boiling liquid, which provides a driving force for heat exchange. The operating principle is nearly identical to vapour compression refrigeration or vapour compression heat pumping systems, but in this case the process fluid is used directly as the heat transfer fluid.

MVC systems in this form provide no direct mechanism for preventing boiling in the main heat exchanger. Evaporation in the heat exchanger can lead to significant deposition of solids or lead to corrosion through increased salt concentration. One potential avenue for

mitigating the fouling caused by boiling is to prevent phase change in the heat exchanger. This is the mechanism through which the advantages of mechanical vapour compression flash distillation (MVC-FD) are based.

The objective of modelling the MVC-FD system is to analyze the effect of pressurizing the fluid in the heat exchanger on overall system operation to determine whether the adjustments cause substantial changes to the overall energy efficiency when the system is used as a desalination process. Further analysis of the impact on scaling needs to be done, but the energy costs should be compared first.

3.2 Modelling Mechanical Vapour Compression Desalination (MVC)

A block flow diagram representing a standard Mechanical Vapour Compression Desalination system and key model variables is shown in Figure 3.1.

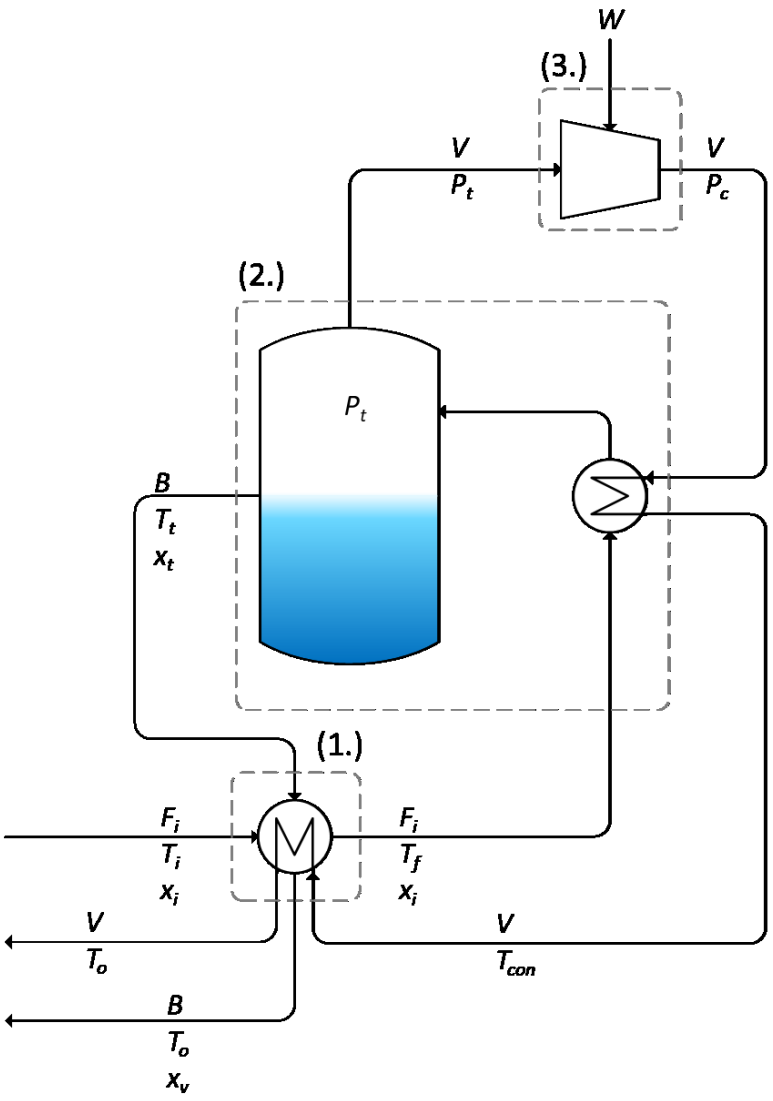

Figure 3.1: Detailed MVC evaporator flow diagram showing key variables and control volumes for steady-state analysis.

The set of equations that make up the steady-state model for the standard MVC desalination system were derived from total mass, component, and energy balances around three control volumes. One set of balances were done around the preheater, which heats feed from temperature T_i to temperature T_f by reclaiming heat from discharged concentrated seawater from the separation vessel, as well as heat from condensate leaving the systems main heat exchanger. An energy balance around the preheater yields:

$$F_i c_{pre} T_i - F_i c_f T_f = -(B c_{Bo} T_o - B c_v T_t) - (V c_{co} T_o - V c_{con} T_{con}) \qquad (2)$$

where F_i, B, and V are the mass flow rates of the feed seawater, the concentrated seawater, and the condensate, respectively, T_{con} is the temperature at which condensate leaves the main heat exchanger, and c_{pre}, c_f, c_v, c_{bo}, c_{co}, and c_{con} are the specific heat capacities of the feed entering the preheater, the feed exiting the preheater, the concentrated seawater, and the condensate exiting the preheater, respectively.

Total mass, component, and energy balances around the second control volume yield equations 3, 4 and 5:

$$F_i = V + B \tag{3}$$

$$F_i x_i = B x_t \tag{4}$$

$$B c_v T_t + V H_t - F_i c_f T_f = V(H_c - H_{con}) \tag{5}$$

where H_t is the specific enthalpy of the steam in the separation vessel, H_c is the enthalpy of the compressed vapour exiting the compressor, and H_{con} is the enthalpy of the condensate leaving the main heat exchanger.

The equations used to model the compressor, represented by control volume 3, are

$$\Delta H_s = H_{cs} - H_{con} \tag{6}$$

$$\Delta H = \frac{\Delta H_s}{\varepsilon} \tag{7}$$

$$H_c = \Delta H + H_t \tag{8}$$

where ΔH_s is the isentropic change in enthalpy across the compressor for a given outlet pressure P_c. Specific enthalpies are evaluated using a steam table look-up function called XSteam (Holmgren, 2007).

The conservation equations were coupled with appropriate physical property models and solved numerically using MATLAB (Mathworks, 2018). The algorithm used to solve the model is shown in Figure 3.2.

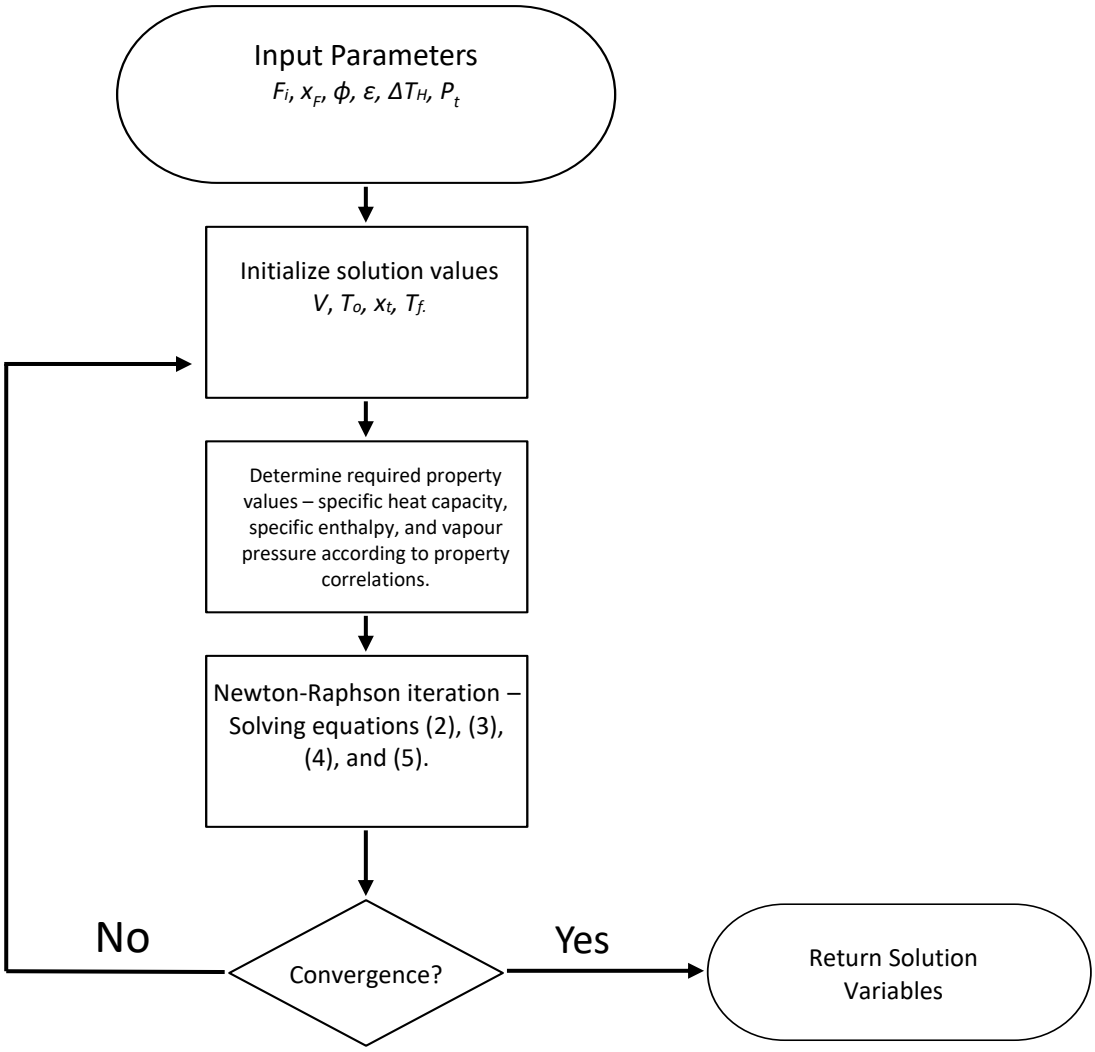

Figure 3.2: Solution procedure for MVC desalination

Input parameters F_i, x_f, ϕ, ε, ΔT_H, and P_t are supplied to the model. These variables are the feed rate, the feed salinity, the recovery of concentrate to feed ratio, and the separation vessel operating pressure. Solution values are initialized. From both the input parameters and initial solution values, properties such as specific heat capacity are computed for all streams. Iterations of the Newton-Raphson method are applied to equations 2-5 until convergence is reached. If convergence is reached, solution variables are returned. If solution values do not yield convergence, the cycle repeats, with the new estimates for solution variables, until convergence is reached.

3.3 Modelling Mechanical Vapour Compression Flash Desalination (MVC-FD)

The MVC-FD model is composed of a system of equations that consists of the series of total mass, component, and energy balances around six control volumes, shown in Figure 3.3, along with some auxiliary relationships. The six control volumes are:

1. Feed and recirculation mixing point
2. Flashing of pressurized recirculation fluid
3. Main heat exchanger
4. Flash tank
5. Steam compressor
6. Preheater

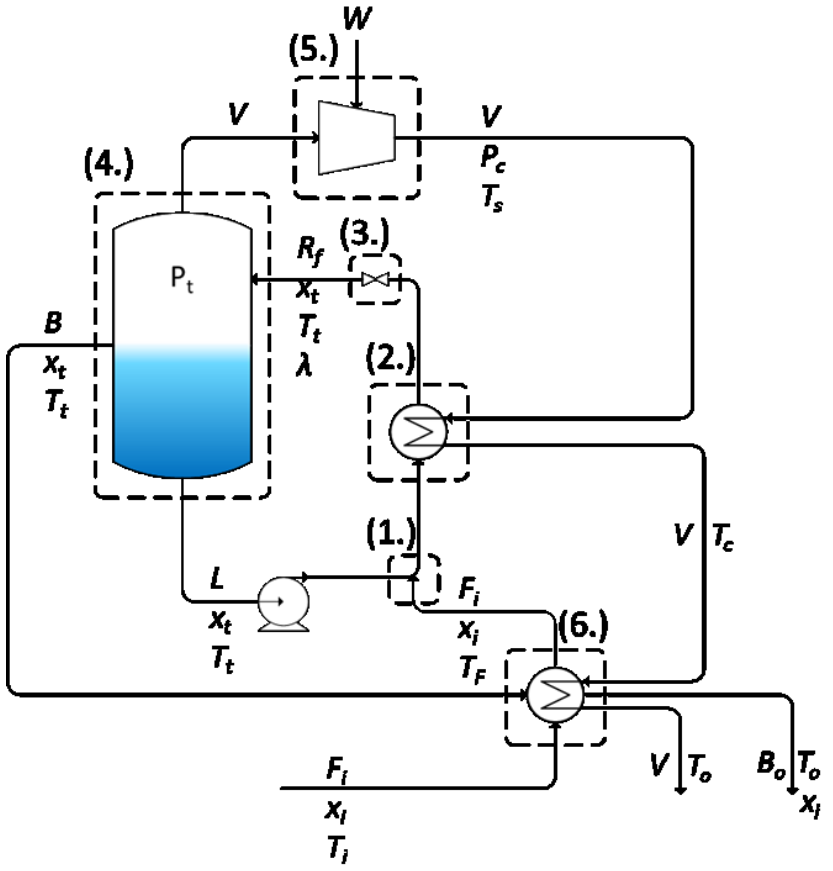

Figure 3.3: Detailed MVC-FD evaporator flow diagram showing key variables and control volumes for steady-state analysis.

The balances around control volume 1 in Figure 3.3 represent the mixing of seawater leaving the preheater with recirculated concentrate. Equation 9 is found by performing a steady-state total mass balance around this mixing point

$$F_i + L = R_i \tag{9}$$

where F_i represents the seawater feed mass flow rate, L represents the recirculation mass flow rate, and R_i is the mass flow rate exiting the mixing point. A component balance around the mixing point at steady-state results in equation 10:

$$F_i x_i + L x_t = R_i x_{ri} \tag{10}$$

where x_i is the salt concentration of the feed, x_t is the salt concentration of the separation vessel, and x_{ri} is the salt concentration of the stream exiting the mixing point (R_i). Equation 11 is derived from the energy balance around the mixing point of the feed and the recirculation loop.

$$F_i c_{fi} T_F + L c_t T_t = R_i c_{Ri} T_{Ri} \tag{11}$$

Mass and component balances around control volume 2 are readily solved because no flows entering are mixed or separated. Equation 12 is acquired by performing an energy balance around control volume 2:

$$R_i c_{Ri} T_{Ri} - R_i c_{Ro} T_{Ro} = V(H_c - H_s) \tag{12}$$

where T_{Ri} and T_{Ro} are the temperature of the feed entering and exiting the tube side of the heat exchanger, respectively, and c_{Ri} and c_{Ro} are the heat capacity of each of these streams, determined from property correlations for seawater as a function of temperature and salt concentration. V is the total steam mass flow rate through the shell-side of the heat exchanger. H_s and H_c are the specific enthalpies of the superheated steam and the saturated condensate entering and leaving the heat exchanger, respectively.

The nozzle, highlighted by balance 3, is modeled as an isenthalpic flash nozzle. The total mass balance is solved readily, but both a component and energy balance are required to determine the phase fractions of the exiting stream and the solids concentration in the liquid stream exiting the nozzle. Total mass and energy balances around the nozzle yield:

$$R_f = R_i \tag{13}$$

$$R_i c_{Ro} T_{Ro} = (1-\lambda) R_f c_{Rf} T_t + \lambda R_f H_t \tag{14}$$

where λ is the steam fraction, H_t is the specific enthalpy of the steam produced through flashing, and c_{Rf} and c_{Ro} are both specific heat capacities of their associated streams, determined through property correlations.

Balances around the separation vessel (4), are used are used to arrive at equations 15 and 16. Two phase balances are done, one for the liquid flow rate and one for the vapour flow rate:

$$\lambda R_f = V \tag{15}$$

$$B + L = (1-\lambda) R_f \tag{16}$$

where B is the mass flow rate of concentrated seawater leaving the separation vessel, L is the recirculation mass flow rate, and C_o is the vapour flow rate leaving the separation vessel.

The balances around control volume (5) involve an isentropic compressor model to determine outlet conditions. The change in enthalpy at constant entropy is determined from equation 17:

$$\Delta H_s = H_{2s} - H_1 \tag{17}$$

where H_{2s} is the enthalpy of the exiting stream at a given exit pressure, P_c, and an entropy equal to the inlet stream. An isentropic efficiency, ε, is applied to ΔH_s according to equation 18 to determine the adjusted change in enthalpy.

$$\Delta H = \frac{\Delta H_s}{\varepsilon} \tag{18}$$

The enthalpy of the exiting stream is then calculated by equation 19. Using the resulting enthalpy and pressure, P_c, conditions for the compressed steam can be found from steam tables.

$$H_2 = \Delta H + H_1 \tag{19}$$

Balances around control volume 6 in Figure 3.3 are used to determine the temperature of the feed entering the recirculation loop. It is assumed that the preheater can be designed such that both the concentrate and condensate streams are cooled to the same temperature, T_o.

$$Bc_{Bt}T_t - Bc_{Bo}T_o + V(H_c - H_o) = -(F_i c_i T_i - F_i c_f T_f) \tag{20}$$

Equations 9 through 20 make up the basis of the MVC-FD model.

SEC is one of the most important parameters for quantifying and comparing the efficiency of a given desalination technology. High SEC leads to increased operating cost. Minimizing SEC is a priority for desalination systems intended to operate for long periods of time. SEC is calculated for the standard MVC model based on equation 21:

$$SEC = (\frac{W}{1000})/(\frac{V}{\rho_w} \cdot 3600) \tag{21}$$

where W is the total work done by the system, V is the product condensate flow rate (produced freshwater), and ρ_w is the density of the distillate produced. SEC for the MVC-FD system is calculated by including the recirculation pumping energy requirements. The specific recirculation pump work is calculated from a modified Bernoulli's equation, arrived at by neglecting energy loss from friction and changes in gravitational potential, shown in equation 22:

$$W_p = \frac{\Delta P_p}{0.75} \tag{22}$$

where ΔP_p is the difference in pressure between the pressure needed to maintain recirculated fluid as a saturated liquid at the outlet of the main heat exchanger, and the pressure at the inlet of the recirculation pump. The value for specific work is then included in the total SEC for the MVC-FD system.

A program was developed in the numerical computing environment MATLAB (Mathworks, 2018), to solve the model. A solution was found for the model, given certain input parameters, according to the algorithm block diagram displayed in Figure 3.4.

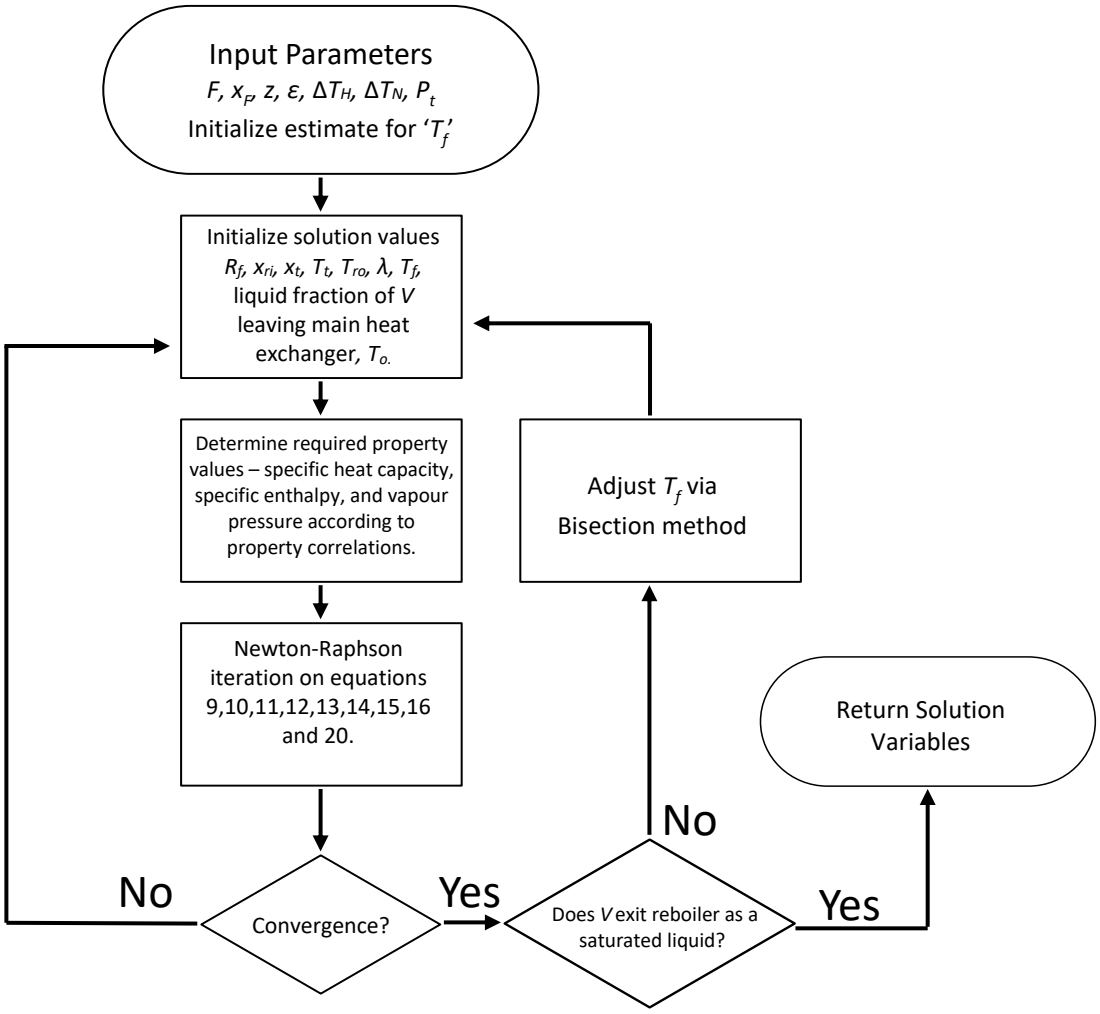

Figure 3.4: Solution procedure for MVC-FD desalination model.

The input parameters are the feed mass flow rate, F, the feed salinity, x_f, the ratio of the recirculation mass flow rate, L, to the feed flow rate, z, the isentropic efficiency of the compressor, ε, the temperature difference across the flash nozzle, the temperature difference between the feed exiting the main heat exchanger and the condensation temperature of steam in the main exchanger, the separation vessel operating pressure, P_t, and the temperature of the condensate and the concentrate leaving the preheater, T_o.

Initial guesses for solution variables are provided so that properties such as specific heat capacity can be calculated; one iteration of the Newton-Raphson method is then applied, and the system of equations is checked for convergence. If convergence has not been reached, the solution variables are updated and the cycle is repeated. If convergence is

reached, the steam condensation fraction is checked. If it is not entirely condensed, T_f is adjusted by using one iteration of the bisection method. This continues until both the system of equations has reached convergence and the fraction of steam condensed in the main heat exchanger is equal to unity. Once both conditions are met, the solution variables are stored.

3.4 Physical Property Correlations and Limitations

In this section, correlations used to calculate property values in both standard MVC and MVC-FD models are discussed. Resulting limitations of the models are discussed where applicable.

The specific heat capacity of the liquid streams in both systems are required for all equations dealing with energy exchange in both system models. In the work by Darwish (1988), constant specific heat capacities were used for all liquid streams for the standard MVC desalination model. In the work presented here, specific heat capacity is calculated as a function of both salt concentration and stream temperature using the correlations presented by Sharqawy et al. (2010). The correlation is

$$c_{sw} = A + BT + CT^2 + DT^3 \tag{23}$$

where

$$A = 5.328 - 9.76 \cdot 10^{-2} S_P + 4.04 \cdot 10^{-4} {S_p}^2$$

$$B = -6.913 \cdot 10^{-3} + 7.351 \cdot 10^{-4} S_P - 3.15 \cdot 10^{-6} {S_P}^2$$

$$C = 9.6 \cdot 10^{-6} - 1.927 \cdot 10^{-6} S_P + 8.23 \cdot 10^{-9} {S_P}^2$$

$$D = 2.5 \cdot 10^{-9} + 1.666 \cdot 10^{-9} S_P - 7.125 \cdot 10^{-12} {S_P}^2$$

where S_p is the salt concentration in g/kg. This correlation was developed from measurements of synthetic seawater for temperatures between 0 and 180°C and salinities ranging from 0 to 180 g/kg (Sharqawy et al., 2010).

Increasing the salt content of water increases its boiling temperature. This phenomenon is referred to as boiling point elevation (BPE). BPE is included in the model by using the equation 24, which is based on Raoult's law (Sharqawy et al., 2010):

$$p_{v,w}/p_{v,sw} = 1 + 0.57357 \cdot \left(\frac{S_P}{1000 - S_P}\right) \tag{24}$$

where $p_{v,w}$ is the vapour pressure of pure water and $p_{v,sw}$ is the vapour pressure of seawater. In conjunction with equation 2, the Antoine equation (Smith et al., 2005) for water, given by equation 25, can be used to calculate the vapour pressure of pure water:

$$\ln(p_{v,w}) = A - \left(\frac{B}{C+T}\right) \tag{25}$$

where $A = 16.2872$, $B = 3885.70$, and $C = 230.17$.

For streams where the properties of steam and liquid water are required, a steam table look-up function called XSteam (Holmgren, 2007) was used. It draws values from the IAPWS IF-97 standard steam table.

The limitations of the correlations in Sharqawy et al. (2010) also become limitations for both MVC and MVC-FD steady-state models. The limits imposed by the property correlations lead to the following restrictions on simulations:

- Salinity of all liquid streams must be between 0 and 180 g/kg
- Liquid streams must be between 0 and 180°C

In addition, the range of data for the IAPWS IF-97 steam table extends from 0 to 1000 bar and from 0 to 2000°C. The upper and lower limits of the range of this table for temperature and pressure are far outside the traditional operating range of MVC systems and as such do not impose limitations on the range of simulations.

3.5 Validation Studies

3.5.1 Comparison with Results of Darwish (1988)

A validation study was done for the MVC model that was developed. Results for system SEC from the model developed in this work were compared with that of Darwish (1988)

for multiple evaporator temperatures. The MVC model input parameters were set to match that of Darwish (1988). The input parameters for the validation case are shown in Table 3.1. The comparison between the results calculated by the model developed here and those found by Darwish (1988) are shown in Figure 3.5. Results from Darwish (1988) have been converted into comparable units (SEC).

Table 3.1: Input Parameters for MVC Validation Case

Feed Rate, F_i (kg/s)	Feed Salinity, x_i (g/kg)	Feed Temperature (°C)	Isentropic Efficiency, ε	ΔT_H (°C)	Evaporator Temperature (°C)	Recovery Ratio (V/F_i)
0.01	42	25	0.70	2-10	50, 70, 90	0.4

ΔT_H is used as a comparison variable in these trials. ΔT_H is defined as the temperature difference between the exit temperature of feed passing through the main heat exchanger and the condensation temperature of pressurized steam supplying heat to the main heat exchanger. For the standard MVC system, the main heat exchanger exit temperature of the feed is also the temperature in the separation vessel. Good agreement is observed between the results by Darwish and those determined from the model developed in this study.

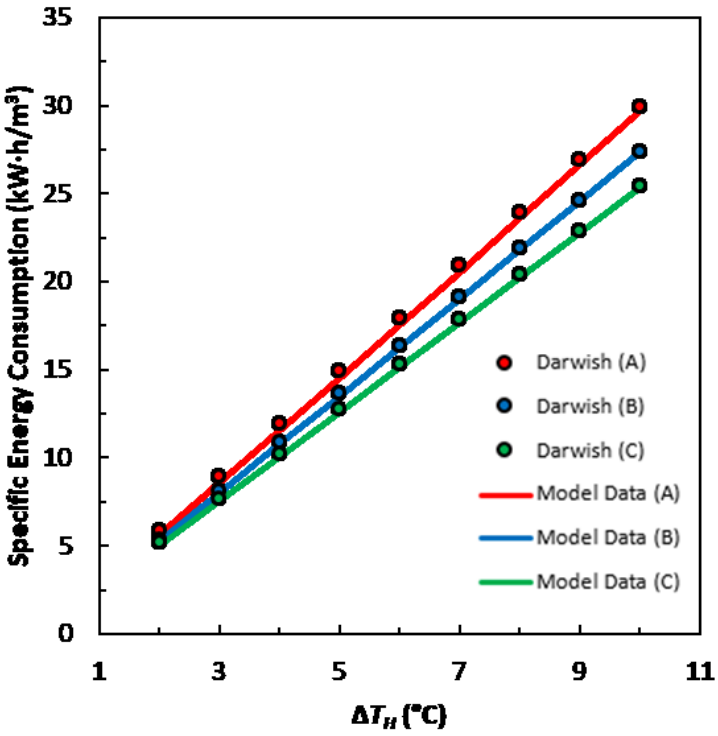

Figure 3.5: System SEC calculated by Darwish (1988) and the MVC model, by ΔT_H and evaporator temperatures (A) 50°C (B) 70°C , and (C) 90°C.

3.5.2 Consistency between MVC and MVC-FD Models

No literature exists on the MVC-FD configuration of the standard MVC system, so it is difficult to compare it to other models. However, the results of the MVC model can be used to validate some aspects of the MVC-FD model. For comparison of the MVC and MVC-FD models an additional variable, ΔT_E, is introduced. ΔT_E is the temperature difference between the separation vessel and the condensation temperature of compressed steam. For the standard MVC system, ΔT_E and ΔT_H have the same value because liquid exiting the main heat exchanger is at the evaporation temperature in the separation vessel. This is not true for the MVC-FD system. For the MVC-FD system, ΔT_E is equal to $\Delta T_H + \Delta T_N$ because the exit temperature of the feed leaving the main heat exchanger is at a temperature higher than the separation vessel to allow for flashing of the liquid passing through the nozzle. For equal values of ΔT_E, the specific energy consumption of the compressor should be the same between MVC and MVC-FD systems, because the compression requirement is the

same at equal values of ΔT_E. Table 3.2 shows the input parameters for the MVC-FD validation case.

Table 3.2: Input Parameters for MVC-FD Validation Case

Feed Rate, F_i (kg/s)	Feed Salinity, x_i (g/kg)	Feed Temperature (°C)	Isentropic Efficiency, ε	ΔT_H (°C)	ΔT_N (°C)	Evaporator Temperature (°C)	Recovery Ratio (V/F_i)
0.01	42	25	0.70	1-10	1,2,3	50	0.4

Figure 3.6 shows a comparison between the compressor SEC requirements calculated by the model for the MVC system and the calculated compressor requirements for the MVC-FD system operated with various ΔT_N values. Across the solid black line in Figure 3.6, the compressor SEC is constant. It is illustrated that for the same ΔT_E value ($\Delta T_N + \Delta T_H$) the SEC requirements of the compressor are equal for both systems. Since the compressor requirements are shown to be the same in the MVC and MVC-FD system models for equal values of ΔT_E, the models are thus shown to calculate compressor requirements consistently.

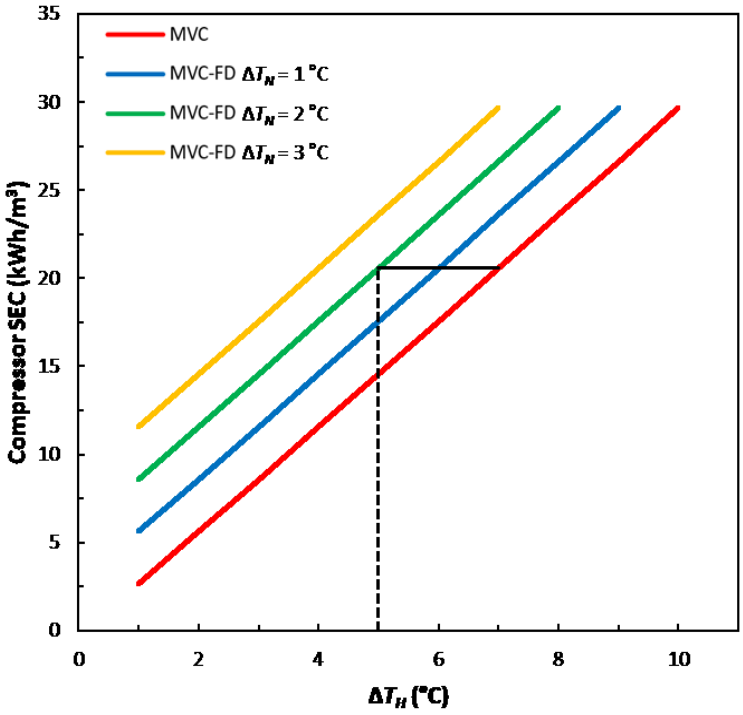

Figure 3.6: Validation simulations for MVC-FD model. Compressor SEC is shown for various ΔT_H values.

3.6 Results and Discussion

Simulations were run for both the MVC and the MVC-FD models. Parameters including Specific Energy Consumption (SEC), compression requirements, and specific heat exchanger area requirements were calculated from the simulations and compared.

3.6.1 Specific Energy Consumption Calculated from MVC and MVC-FD Process Models

Figure 3.7 shows the calculated SEC as a function of ΔT_H for the standard MVC system. For the standard MVC system, the exit temperature of the feed from the main heat exchanger is also the temperature in the separation vessel. Trends are shown for separation vessel operating pressures (P_t) of 50, 70, and 100 kPa. The recovery ratio is set to 0.5 (defined as the ratio of distillate rate to feed rate) for all simulations shown. Simulation input parameters are listed in Table 3.3.

Table 3.3: Simulation Parameters for MVC SEC and Compression Results

Feed Rate, F_i (kg/s)	Feed Salinity, x_i (g/kg)	Feed Temperature (°C)	Isentropic Efficiency, ε	ΔT_H (°C)	Pressure P_t (kPa)	Recovery Ratio (V/F_i)
0.01	35	25	0.75	1-10	50, 70, 100	0.5

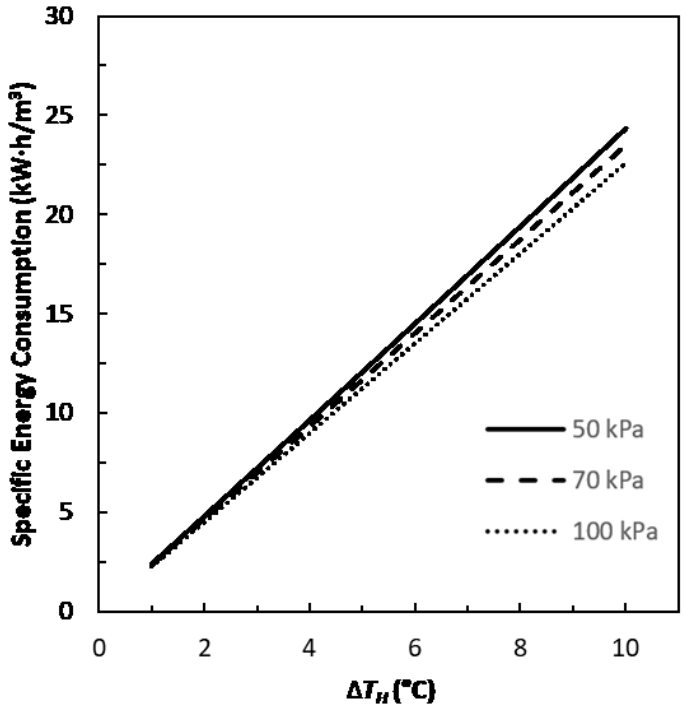

Figure 3.7: Results of MVC model for desalination

As shown in Figure 3.7 the SEC of a standard MVC system is strongly dependent on ΔT_H. To achieve higher ΔT_H, the steam condensation temperature must increase. The compressor outlet pressure must increase to achieve this, resulting in higher energy demand.

The operating pressure of the separation vessel also has a notable impact on SEC. As shown in Figure 3.7, the SEC decreases as the operating pressure of the separation vessel increases. This is counter-intuitive because higher operating pressures require a higher change in pressure across the compressor, which increases the SEC. However, increasing the operating pressure also reduces the specific volume of the steam, thereby reducing SEC.

These two effects counter-balance each other, with the net result being a reduction in SEC as operating pressure is increased (Darwish, 1988).

Figure 3.8 presents simulation results showing the effect of ΔT_H on the SEC for various separation vessel operating pressures over different values of ΔT_N. ΔT_N is the temperature difference across the flash nozzle. Input parameters are listed in Table 3.4.

Table 3.4: Simulation Parameters for MVC-FD SEC and Compression Results

Feed Rate, F_i (kg/s)	Feed Salinity, x_i (g/kg)	Feed Temperature (°C)	Isentropic Efficiency, ε	ΔT_H (°C)	ΔT_N (°C)	Pressure P_t (kPa)	Recovery Ratio (V/F_i)
0.01	35	25	0.75	1-10	0.5, 3 ,5	50, 70, 100	0.5

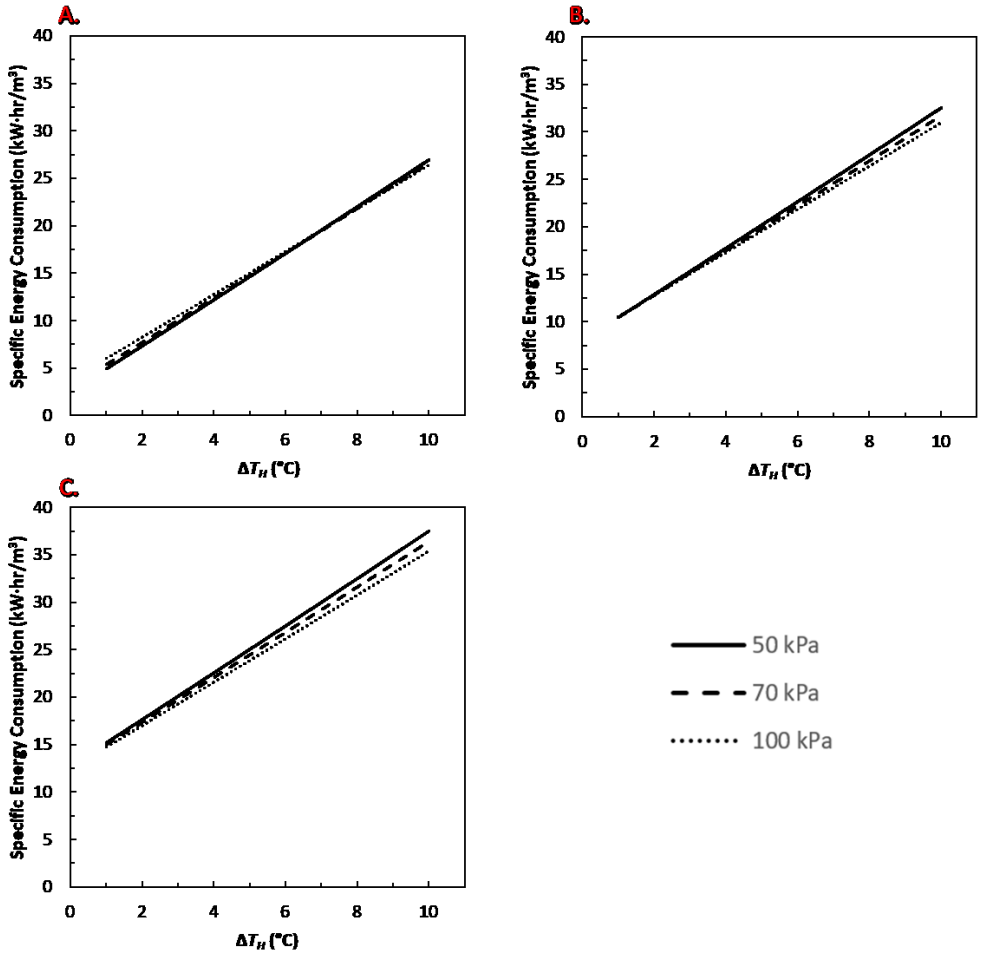

Figure 3.8: SEC of MVC-FD systems for various ΔT_N and ΔT_H values. A: ΔT_N of 0.5, B: ΔT_N of 3, C: ΔT_N of 5.

Specific recovery ratios are reached in MVC-FD by adjusting two operating variables: either the recirculation rate, L, or ΔT_N. For a given recovery and ΔT_N, a specific recirculation value is required. This occurs because both ΔT_N and L impact the total enthalpy of the feed passing through the flash nozzle, and thus affect the total sensible heat available for flashing. These operational variables are not present in the standard MVC system and thus play a role in the differences between standard MVC and MVC-FD simulation results.

As shown in all three figures for the MVC-FD simulations, as ΔT_H increases the SEC also increases. This is the same general trend seen in standard MVC desalination simulations. This trend is caused by the higher ΔP requirement across the compressor caused by increased values of ΔT_H. Higher ΔT_H values increase ΔP because as the temperature of condensation increases on the steamside of the main heat exchanger, a higher pressure is required. Additionally, as ΔT_N is increased, the SEC increases, as is shown by Figure 3.8. This happens for the same reason that an increase in ΔT_H increases the SEC. The temperature difference between the separation vessel and the condensation temperature of the steam is the sum of ΔT_H and ΔT_N. Larger values of either parameter require an increase in ΔP across the compressor as shown in Figure 3.8. Table 3.5 shows values for the SEC for different values of ΔT_N and ΔT_H, for the input parameters listed in Table 3.4. Table 3.5 better presents the numerical impact that increasing both ΔT_H and ΔT_N has on the SEC.

Table 3.5: SEC for MVC and MVC-FD Simulations

	Specific Energy Consumption (kWh/m^3)			
	MVC	**MVC-FD**		
ΔT_H		ΔT_N **= 0.5 °C**	ΔT_N **= 3**	ΔT_N **= 5 °C**
1	2.38	4.97	10.45	15.20
3	7.21	9.80	15.32	20.10
5	12.1	14.67	20.22	25.03
7	16.95	19.56	25.14	29.99
10	24.33	26.95	32.59	37.47

The benefits of operating at a higher ΔT_N is a reduction in pumping requirements. This is more evident in Figure 3.9, which shows the impact of ΔT_N on pumping requirements.

Increasing ΔT_H reduces pump power consumption. The benefits of increasing ΔT_N are minimal. This is shown in Table 3.5 where increasing ΔT_N still results in higher SEC consumption, despite lower pumping requirements. The impact of the increased compression requirements on the SEC offset any potential benefit of reducing pumping requirements with respect to energy usage. Lowering the recirculation rate requirements by increasing ΔT_N may reduce capital costs, e.g. by reducing the piping requirements, but quantifying these benefits has not been made an objective of this work.

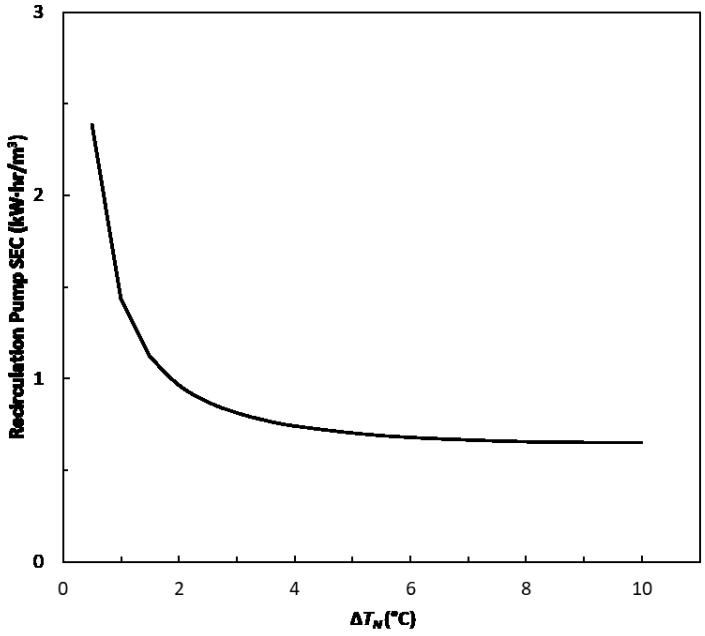

Figure 3.9: Recirculation Pump contribution to total SEC by ΔT_N for MVC-FD simulation at 50 kPa and ΔT_H of 3.

The addition of the ΔT_N parameter causes a difference between MVC-FD and MVC desalination with respect to SEC. When small ΔT_N values are used, increased operating pressure also increases the SEC at low values of ΔT_H. As ΔT_N is increased, the relationship between the SEC and the operating pressure approaches the trend present in standard MVC systems.

3.6.2 Compression Requirements Calculated from MVC and MVC-FD Process Models

A key parameter when sizing systems involving compressors is the pressure difference (ΔP) required across the compressor. Larger pressure differences require more specialized equipment, which increases capital investment. Simulations were performed to determine ΔP requirements for both standard MVC and MVC-FD systems as a function of ΔT_H. These results are presented in Figure 3.10 and Figure 3.11 for MVC and MVC-FD, respectively.

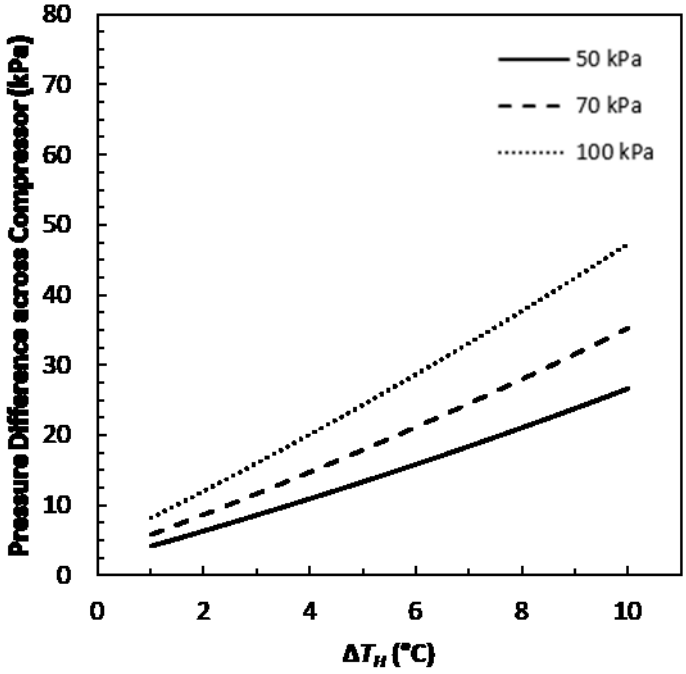

Figure 3.10: Compression requirements for standard MVC as a function of ΔT_H.

The pressure difference requirements of the compressor are determined primarily by two variables: ΔT_H and P_t. Increasing either one of these variables leads to higher compression requirements. Compressors that operate at a higher compression ratio are more expensive, thus lower compression requirements are desired.

The ΔT_H for standard MVC desalination is defined as the difference in evaporation temperature in the main heat exchanger and the compressed steam condensation temperature. As this difference is increased, the pressure at the outlet of the compressor

must increase relative to the separation vessel pressure to maintain condensation at the designated temperature, which results in higher compression requirements. As P_t increases, larger pressure differences are required to maintain the same difference between the evaporation and condensation temperatures of the brine and the compressed steam.

Figure 3.11 displays the effect of ΔT_H for the MVC-FD system for ΔT_N values of 0.5, 3 and 5. The impact of increasing ΔT_H or P_t on compression requirements for MVC-FD systems is similar to that seen in the standard MVC desalination system. Increasing ΔT_H increases the steam condensation temperature, leading to higher compression requirements. At higher values of P_t, the impact of increasing ΔT_H becomes more significant.

MVC-FD systems operated with low values of ΔT_N have compression requirements like those of standard MVC desalination systems. This is shown in Figure 3.12, which combines Figure 3.10 and Figure 3.11A.

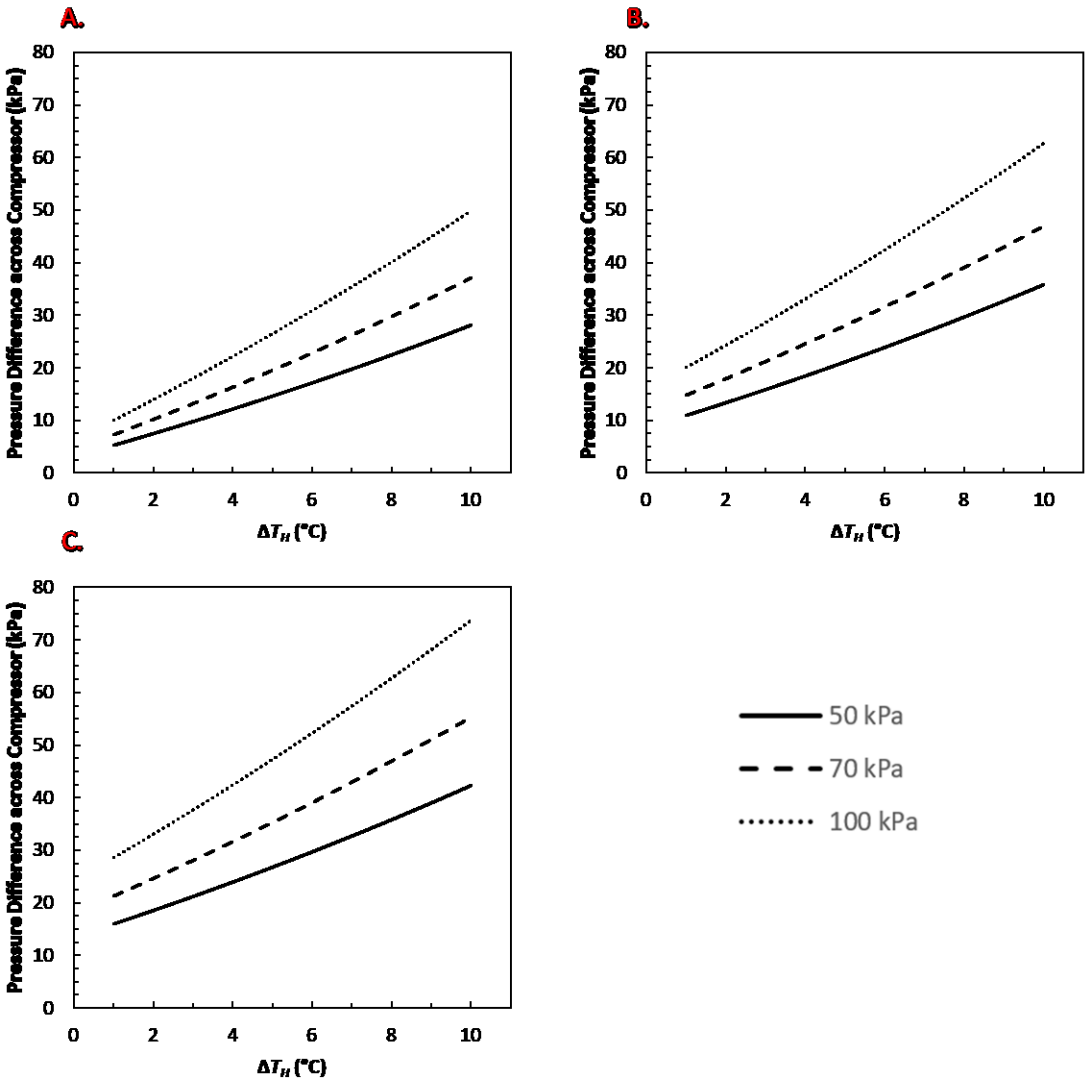

Figure 3.11: Compression requirements for varying ΔT_H. A: ΔT_N of 0.5, B: ΔT_N of 3, C: ΔT_N of 5, for MVC-FD system.

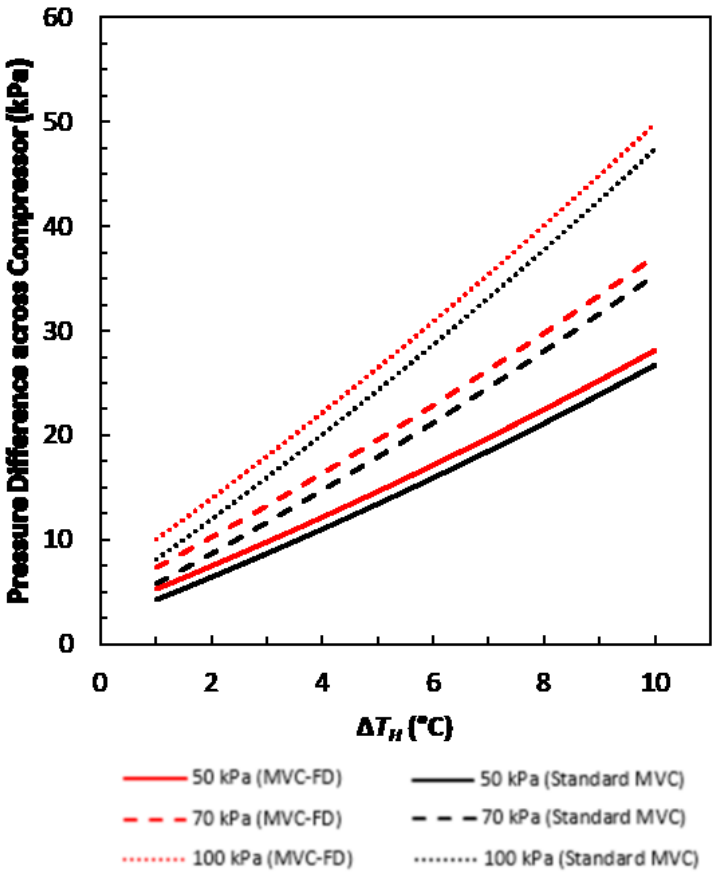

Figure 3.12: Comparison of standard MVC and MVC-FD compression requirements.

The increase in compression requirements for MVC-FD relative to standard MVC desalination is between 5 and 10%, when operating at a ΔT_N below 0.5, and at a ΔT_H above 4. Operating MVC-FD at higher ΔT_N leads to significant increases in compression requirements. Increasing ΔT_N to a value of 3 yields a difference in compression of between 30 and 75% for the same ΔT_H. ΔT_N should be kept low to limit increases in compression requirements.

3.6.3 Specific Heat Exchanger Area Requirements Calculated from MVC and MVC-FD Process Models

The final major piece of equipment associated with both systems is the main heat exchanger used to heat the feed prior to the separation vessel. Simulations were performed to determine specific area requirements for both systems. Specific area is defined as the

ratio of the heat exchanger area required to the volume of distillate produced. The equation used to determine specific area is shown in equation 26:

$$A_s = \left(\frac{Q_s}{U_o \cdot \Delta T_{lm}}\right)/V \tag{26}$$

where A_s is the area divided by the distillate flow rate, Q_s is the total energy exchanged across the surface of the heat exchanger, ΔT_{lm} is the logarithmic average temperature difference, V is the total distillate flow rate, and U_o is the overall heat transfer coefficient.

Due to the different operating conditions of the MVC and MVC-FD systems, it is difficult to directly compare them with specific heat exchanger designs and their associated heat transfer coefficients. The optimal heat exchanger design is different for each system. As such, a value for the overall heat transfer coefficient, U_o, was selected for comparison purposes, with the assumption that for each real system it is possible to design a heat exchanger that meets the chosen U_o value under the conditions present for each system. The issue with this type of analysis is that it does not capture the influence of different operating conditions on U_o. For example, changes in operational parameters such as ΔT_N in the MVC-FD system can have significant impacts on fluid flow through the heat exchange equipment, reducing convective heat transfer coefficients, and by relation, U_o. Under some non-optimal operating conditions, it may not be possible to achieve the overall heat transfer coefficient recommended. This type of comparison is not included in this analysis.

From Sinnott (2005), overall heat transfer coefficient values are said to generally range from 1500 to 4000 W/(m^2 °C) for heat exchangers in which steam acts as the hot fluid and water acts as the cold fluid. From this, the lower value of 1500 W/(m^2 °C) was selected as the basis of simulations to account for potential difficulty in achieving high heat transfer coefficient values in a real design. ΔT_E is the difference between the temperature at which liquid in the separation vessel evaporates and the temperature at which compressed steam condenses in the main heat exchanger. Figure 3.13 presents the specific heat exchanger area requirements for a standard MVC desalination system and for a MVC-FD system, for different values of ΔT_E for systems designed to achieve an overall heat transfer coefficient

of 1500 W/(m^2 °C). Multiple MVC-FD simulations are shown, differentiated by their respective ΔT_N values.

ΔT_E is chosen as the dependent value in the heat exchanger comparison because standard MVC desalination systems operating with the same ΔT_E as MVC-FD require the same amount of compression to achieve steady state, putting the two systems on equal ground. In addition, since the compression is the same for both systems, so is the specific energy consumption of the compressor.

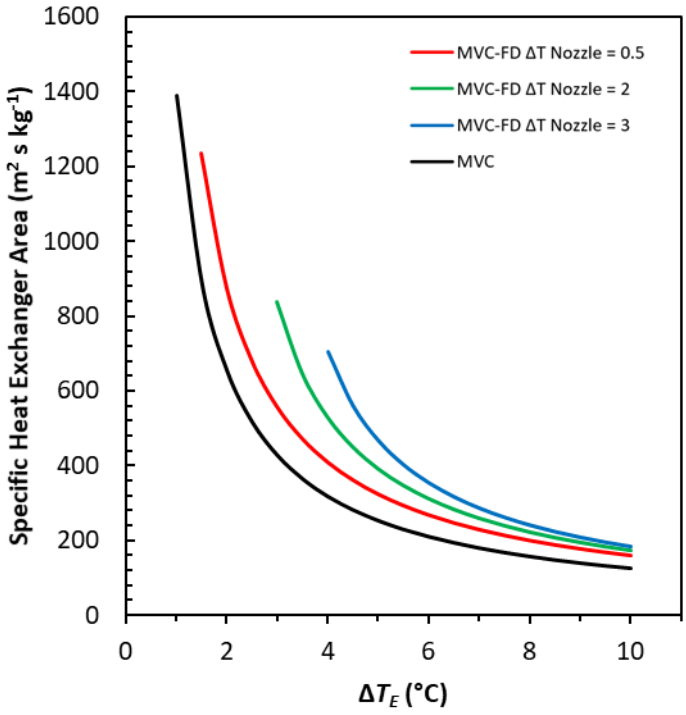

Figure 3.13: Specific heat exchanger area requirements for MVC and MVC-FD systems. Simulations are run at 0.5 recovery ratio and 70 kPa operating pressure.

The MVC-FD system requires larger heat exchanger areas than the standard MVC desalination system for most values of ΔT_E. Values of ΔT_E greater than 12 show convergence of specific area requirements, though operating at these values leads to SEC requirements that are significantly above those of other desalination technologies and should thus be avoided. Increasing the ΔT_N value for the MVC-FD system leads to higher specific heat exchanger area requirements for most values of ΔT_E. This trend begins to

vanish at higher ΔT_E values, but these values are outside the range of ΔT_E values that would be used during real operation.

When ΔT_N is at a value of 0.5, the MVC-FD system requires an approximately 60 to 20% increase in specific heat exchanger area relative to the MVC system for ΔT_E values ranging from 2 through 10. This is quite a significant increase, and large benefits in terms of reduced fouling would be required to offset this cost. Increasing the outlet compressor pressure on the MVC-FD system would reduce the heat exchanger size to make it more comparable to that of the MVC system, but this would be at the cost of increasing the SEC.

3.6.4 Summary

The SEC of the MVC and MVC-FD systems were modelled. It was shown that the requirement of a temperature change across the flash nozzle (ΔT_N) significantly increased the SEC of the MVC-FD relative to MVC systems. Reducing the ΔT_N value was shown to reduce the SEC of the MVC-FD system, and make it more comparable to that of the standard MVC system. By limiting the ΔT_N value, the increased SEC and additional compression requirements of the MVC-FD system can be made insubstantial. The heat exchanger requirements of the MVC-FD system significantly increased in comparison with those of the standard MVC system, when operated under the same ΔT_E value. MVC-FD heat exchanger requirements are shown to be greater than 20% higher than those calculated for the standard MVC system.

Chapter 4

Fouling in MVC and MVC-FD Evaporator Systems

The objective of this section is to examine the differences in fouling potential between the MVC evaporation system and the proposed MVC-FD system during operation. The comparison is made by processing two different fluid systems: NaCl-$CaSO_4$-H_2O and NaCl-H_2O. The intention is to illustrate the potential of the MVC-FD to inhibit the formation of conditions which promote precipitation in heat exchanging equipment. This is done by determining maximum fouling potential.

The principle by which the MVC-FD reduces fouling of heat exchange surfaces is by preventing evaporation on heat exchanging surfaces, and instead moving the evaporation to an area of the system more suitable for handling solids precipitation (across the flash nozzle). This prevents liquid volume change from increasing the dissolved solids concentration past the solubility limit at heat exchange surfaces, and thus preventing conditions that lead to precipitation (Wittering, 2015). Since there are many operations requiring the evaporation of fluids that may contain potentially fouling dissolved salts, the MVC-FD system is applicable to a wide range of operations outside of desalination.

To examine the benefits of MVC-FD over standard MVC evaporation, a fouling model was constructed for both systems such that relative fouling potential could be compared for a given process fluid. Many different types of scale can form due to precipitation in multi-component fluids (Singh et al., 2017). To develop a tractable model, scaling potential is evaluated in this study for systems with a single fouling component.

For building fouling models to compare the MVC and MVC-FD systems, an analogue solution to seawater was selected to reduce complexity. $CaSO_4$ and $CaCO_3$ are the most widely reported fouling compounds in seawater, so therefore the choice was made between model based on processing either a NaCl-$CaCO_3$-H_2O solution or a NaCl-$CaSO_4$-H_2O solution. The solubility trends for $CaSO_4$ and $CaCO_3$ are similar. The solubility limits of both compounds decrease with increasing temperature in saline water, while with increasing salinity the solubility of both compounds increases (Seidell, 1919). However,

the most important factor in determining the solubility of $CaCO_3$ is the dissolved CO_2 content in solution (due to its effect on pH), whereas $CaSO_4$ solubility is independent of pH. Due to the added requirement of tracking pH with the NaCl-$CaCO_3$-H_2O system, the NaCl-$CaSO_4$-H_2O system was chosen for modelling.

4.1. Modelling Fouling with a NaCl-$CaSO_4$-H_2O system in MVC and MVC-FD Evaporators

The objective of this section is to describe the development and implementation of a fouling model for mixtures of NaCl-$CaSO_4$-H_2O to predict the relative maximum fouling potential of MVC-FD and standard MVC evaporation systems.

Rate-based fouling models are much more accurate in predicting the likeliness of precipitation of dissolved solids at heat exchanging surfaces. However, they require multiple additional parameters that were neither included nor within the capacity of the previously developed MVC evaporation and MVC-FD steady-state models to calculate. A rate-based model specifically designed to calculate numerous additional parameters would be needed, such as in the work by Esawy et al. (2017). The applicability of such models is limited to the geometries for which they were developed. A fouling model that examines bulk fluid solubility and determines the maximum fouling potential based on degree of supersaturation does not have these limitations, and thus is more straightforward to implement within the structure of the developed process models.

Calcium sulfate can precipitate out of water solutions in three phases, each differentiated by a different degree of hydration. These three phases are anhydrite ($CaSO_4$), hemihydrate ($CaSO_4 \cdot 0.5H_2O$), and gypsum ($CaSO_4 \cdot 2H_2O$) which is also known as dihydrate (Freyer, 2000). The phase diagram for the $CaSO_4$-H_2O system, displayed in Figure 4.1, shows the solubility of calcium sulfate for given solution conditions.

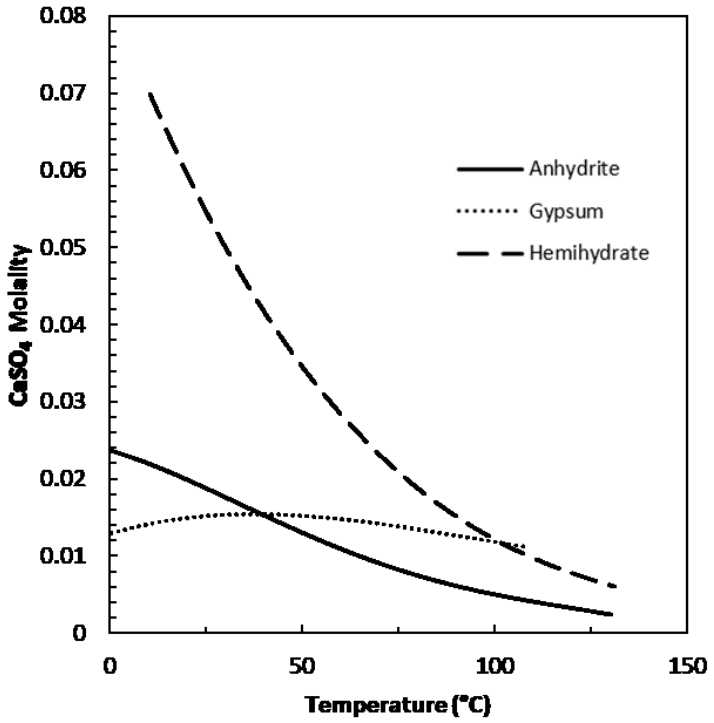

Figure 4.1: Phase diagram for $CaSO_4$ system. Data from Azimia et al. (2007)

From Figure 4.1 it can be determined that for most temperatures, the stable phase that forms from dissolved calcium sulfate is anhydrite. Gypsum is the most stable phase up until around 42 to 50°C. The transition temperature of the stable phase between gypsum and anhydrite is disputed but in most literature it is accepted to be at the lower end of this range, at approximately 42 to 46°C (Van Driesseche et al., 2017). Calcium sulfate anhydrite is the most stable form in the temperature range of interest in MVC-FD and MVC operations (25-110°C).

Solubility models and measurements for calcium sulfate salt solutions have been constructed in multiple works. Work by Power et al. (1966) provided solubility data, and from that solubility data created a model to calculate the solubility and phase stability of calcium sulfate in water for various temperatures and sodium chloride (NaCl) concentrations. The model of Power et al. (1966) computes the solubility of anhydrite from equation 27, where K^o is the solubility product for calcium sulfate, m is the molality of calcium sulfate at its maximum solubility, and γ is the mean activity coefficient of calcium sulfate (Power et al., 1966):

$$K^o = m^2\gamma^2 \tag{27}$$

γ is calculated from equation 28, where D is the dielectric constant of water, T is the absolute temperature, μ is the ionic strength of solution.

$$\log \gamma_{CaSO_4} = \frac{[(7.296\ X\ 10^6)/(DT)^{\frac{3}{2}}]\ (\mu)^{1/2}}{1 + \frac{A}{(DT)^{1/2}}\ (\mu)^{1/2}} \tag{28}$$

Values for D and $A/(DT)^{1/2}$ over a range of temperatures are tabulated by Power et al. (1966). A regression curve was generated to fit this data, which allowed values to be computed across the range of temperatures required in the model. A polynomial was fit to the data provided by Power et al. (1966) for the average K^o by temperature. Using this polynomial for K^o and equations 27 and 28, and the developed polynomial relationships for D and $A/(DT)^{1/2}$, the solubility of calcium sulfate anhydrite can be calculated. Results from the implemented model are provided in Figure 4.2 and compared with the data from Power et al. (1966) This implementation of the model has good agreement with the data from Power et al. (1966).

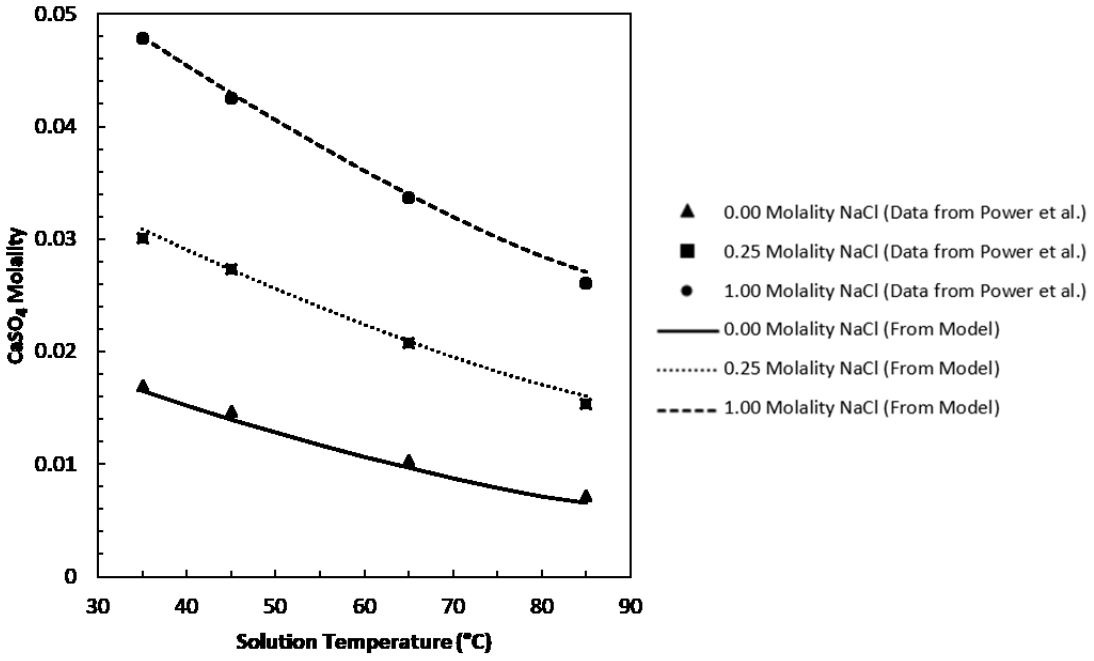

Figure 4.2: Solubility of $CaSO_4$ (anhydrite) - Model Comparison with data from Power et al. (1966).

The steady-state MVC and MVC-FD process models were used in conjunction with this solubility model to predict the tendency toward precipitation and scaling of heat exchanging devices in these two systems. To implement the solubility model, two main changes were required:

- Implementation of variables to track stream concentration of calcium sulfate
- Addition of mass balances associated with the fouling component across heat exchanging devices and flash valves.

Around the preheater, a component balance shown in Equation 29 is added to allow for tracking of calcium sulfate concentration. This is done for both MVC and MVC-FD systems.

$$\tau = F_i x_{i_{CaSO4}} - F_o x_{o_{CaSO4}} \tag{29}$$

In Equation 29, $x_{i_{CaSO4}}$ and $x_{o_{CaSO4}}$ are the concentrations of calcium sulfate in the streams, and F_i and F_o are the total mass flow rates entering and exiting the preheater, respectively. The maximum solubility of calcium sulfate is calculated for the exit stream based on temperature and salinity. The parameter τ represents the amount of calcium sulfate that must precipitate for the solution to reach saturation. As such, it is used is to identify the maximum fouling potential of the heat exchanger. If the maximum solubility is higher than $x_{o_{CaSO4}}$, then τ is equal to 0; otherwise, τ is calculated from equation 29, by assuming $x_{o_{CaSO4}}$ is equal to the maximum solubility derived from the previously described solubility model. Total mass balances and energy balances were adjusted to account for the change in mass flow across both heat exchangers in each steady-state model, and for the balances across the nozzle in the MVC-FD model. Similar adjustments were made to the balances done around the main heat exchanger in both models, and the balances around the flash nozzle in the MVC-FD model.

4.1.1 Results for Precipitation for NaCl-$CaSO_4$-H_2O System

Simulations were performed for both systems to estimate the maximum potential rate of fouling for the MVC and MVC-FD systems, processing NaCl-$CaSO_4$-H_2O solution saturated with $CaSO_4$. This fluid was selected to give an indication of the maximum

potential fouling in each of the two systems when processing a fluid containing a fouling component that has both a decreasing solubility with temperature and an increasing solubility with the concentration of a secondary component (Power et al., 1966).

The MVC-FD system is intended to reduce fouling potential by preventing phase change in the heat exchange equipment and allowing the phase change to occur in areas of the system that can handle solids fouling. Phase change occurs after the pressurized process fluid passes through the flash nozzle due to superheating. In a real system, a solids collection device such as a filter or a cyclone would be present either in the separation vessel or in the recirculation loop. The analysis regarding the solids collection device has not been included in the review of this system. For modelling purposes, solids that precipitate across the nozzle are considered to be removed from the system.

Simulations were run for MVC-FD and MVC evaporator systems processing NaCl-$CaSO_4$-H_2O. Simulation input parameters were set at a tank pressure of 50 kPa, with the feed process fluid having an NaCl content of 4 g/kg, and saturated with dissolved $CaSO_4$. Additionally, the temperature difference between the outlet and the compressed steam inlet to the main heat exchanger was set to 10°C. For the MVC-FD system, this temperature difference was split so that there was a 5°C temperature difference across the flash nozzle, and a 5°C temperature difference between the outlet of the heat exchanger and the compressed steam inlet. The maximum potential fouling rates predicted for the system run with these input parameters are shown in Figure 4.3 as a function of recovery.

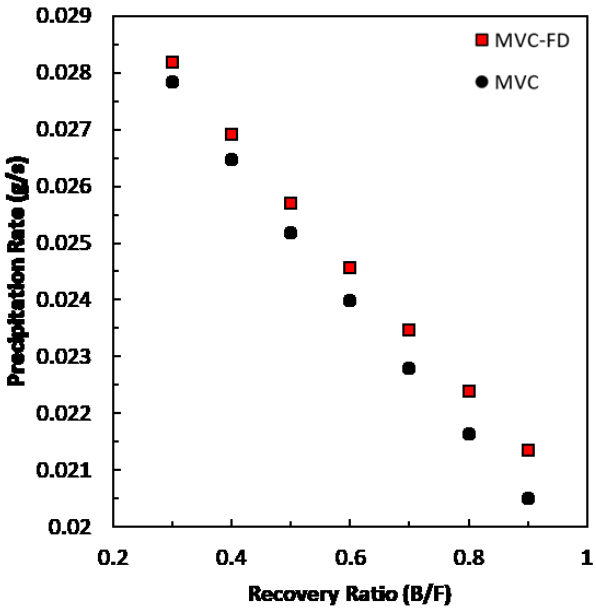

Figure 4.3: Total predicted precipitation rate for MVC-FD and MVC evaporator systems for processing NaCl-H_2O-$CaSO_4$ fluid through heat exchanging equipment.

As can be seen from Figure 4.3, more fouling occurs in the MVC-FD system than in the standard MVC evaporator. Across the range of recovery values shown, the potential precipitation rate predicted by the model increases by 1 to 5%. Additionally, no solids are precipitated across the flash nozzle in the MVC-FD system. The predicted maximum precipitation rate across heat exchanging equipment is similar in each system, which demonstrates that the MVC-FD has failed to inhibit conditions that lead to the formation of scale.

The solubility trends of $CaSO_4$ are instrumental to understanding the failure of the MVC-FD system to reduce fouling conditions, despite preventing phase change in the main heat exchanger. According to the solubility model, two parameters directly affect the maximum solubility of $CaSO_4$ in the MVC-FD system. These parameters are the temperature of the solution, and the concentration of NaCl. The precipitation of calcium sulfate is also affected by the evaporation of water which both concentrates $CaSO_4$ past its solubility limit and concentrates NaCl, which impacts maximum solubility.

The temperature at the outlet of the main heat exchanger is higher in the MVC-FD system for all trials run. This reduces the solubility of $CaSO_4$ and increases the precipitation of solids to levels greater than that found in the MVC evaporator system. Effectively, the solids precipitation resulting from temperature change alone is greater in the MVC-FD system. Main heat exchanger outlet temperatures are illustrated for both MVC and MVC-FD model results in Figure 4.4.

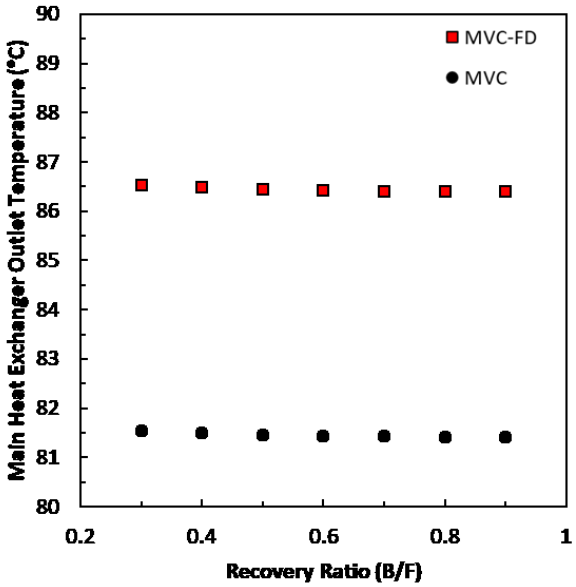

Figure 4.4: Main heat exchanger outlet temperatures for MVC and MVC-FD systems

No solids are predicted to precipitate across the flash nozzle in any trial. Across the nozzle, the liquid volume is reduced, which should encourage solids precipitation. However, other changes in solution conditions also occur across the flash nozzle, such as a reduction in temperature, and an increase in NaCl content (due to evaporation). These two changes increase the solubility of calcium sulfate in solution. Since no precipitate is formed across the flash nozzle, the impact of the salinity increase and the temperature drop on solubility must be overcoming any change in solubility caused by the reduction in liquid volume across the flash nozzle.

In the case of processing a solution composed of NaCl, $CaSO_4$, and H_2O, where $CaSO_4$ acts as the fouling component, the MVC-FD system increases fouling potential, because

its solubility trends did not allow for precipitation across the flash nozzle and resulted in precipitation across the heat exchanger caused by a phenomenon other than liquid volume change.

4.1.2 Modelling and Results for Precipitation with a NaCl-H_2O System

It has been shown that the MVC-FD evaporator does not reduce fouling potential for the NaCl-$CaSO_4$-H_2O system, where calcium sulfate is the fouling compound. This result gives an indication as to how the MVC-FD handles foulants where precipitation is not driven primarily by liquid volume change.

An additional fluid system was analyzed to illustrate the effectiveness of the MVC-FD system for processing fluid with a fouling component that has properties differing from the NaCl-H_2O-$CaSO_4$ system. The solubility curve for NaCl in water is shown in Figure 4.5, compiled from data from Seidell (1919).

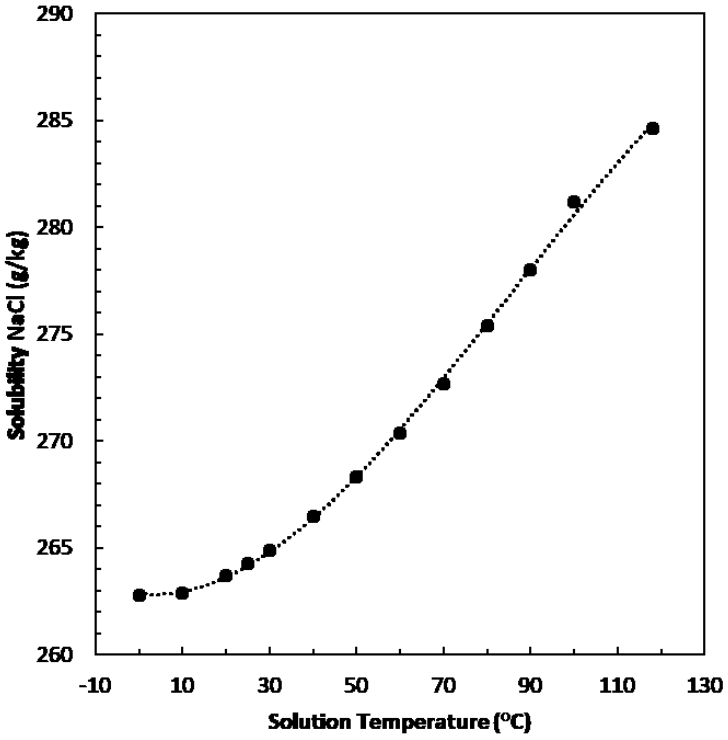

Figure 4.5: Solubility curve for sodium chloride in water. Data from Siedell (1919).

As shown in Figure 4.5, as temperature increases, the solubility of sodium chloride increases. Modelling the maximum potential precipitation of NaCl gives some insight into the relative fouling potential of the MVC-FD system and of the MVC evaporator, where temperature increases alone do not cause precipitation.

Simulations were run for MVC and MVC-FD evaporators processing water saturated with NaCl, for different recovery values. Figure 4.6 shows the maximum potential precipitation rate of NaCl, calculated from changes in bulk composition and solubility, across both the preheater and main heat exchanger of the MVC evaporator on the feed side.

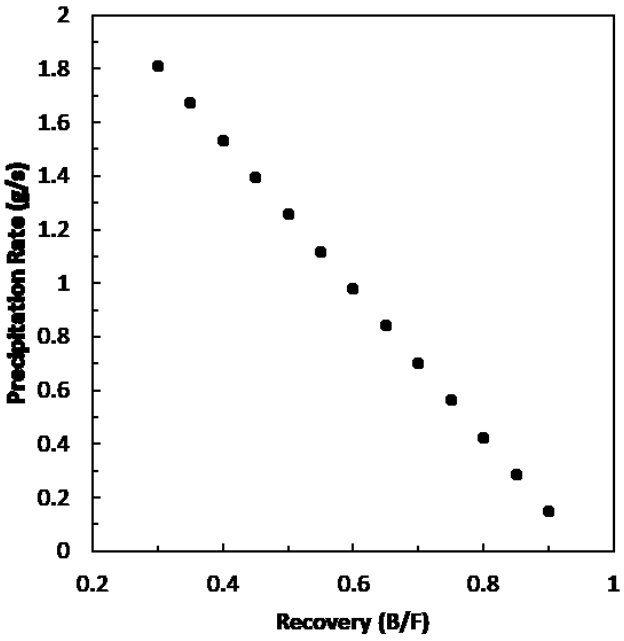

Figure 4.6: Precipitation rate of NaCl in the MVC evaporator configuration

As more fluid is evaporated, more NaCl precipitates. All the precipitation from the feed stream occurs in the main heat exchanger. As feed passes through the preheater, the solubility of sodium chloride increases as the temperature of the solution rises, preventing its precipitation. It is only in the main heat exchanger, where change in liquid volume occurs, that solids can precipitate. At high recovery ratios (small changes in liquid volume), the increase in temperature is high enough to inhibit precipitation brought on by liquid evaporation.

For the MVC-FD system, no precipitation of NaCl occurs on the feed side of the preheater and the main heat exchanger. However, precipitation of NaCl does occur across the flash nozzle. Figure 4.7 shows the comparison between the precipitation rate of NaCl across the flash nozzle in the MVC-FD system, and the precipitation rate of NaCl in the main heat exchanger of the MVC evaporator.

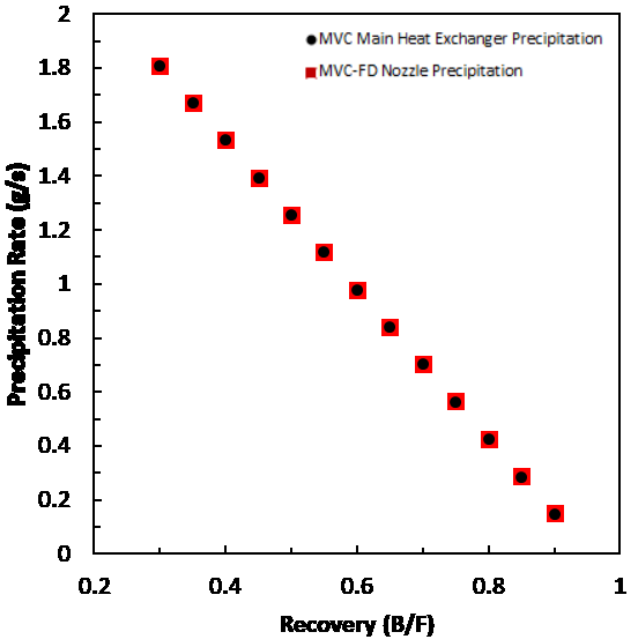

Figure 4.7: Solids precipitation comparison across the flash nozzle in the MVC-FD evaporator and across the main heat exchanger in the MVC evaporator.

The solids precipitation rate across the flash nozzle in the MVC-FD evaporator system matches that found across the main heat exchanger of the MVC evaporator. This should be expected because the main driver of NaCl precipitation is liquid volume change in both systems.

4.2 Summary

The precipitation of solids was examined using a bulk solubility approach for both MVC and MVC-FD evaporators. Solubility models were developed for two fluid systems based on available data. Used in conjunction with the previously developed MVC-FD and MVC steady-state evaporator models, estimates for maximum potential precipitation rates at

steady-state were made. Maximum fouling potential in the MVC-FD and MVC evaporator systems were compared. The fluid systems that were examined were NaCl-$CaSO_4$-H_2O and NaCl-H_2O. $CaSO_4$ is considered the fouling compound in the NaCl-$CaSO_4$-H_2O fluid system. NaCl is considered the fouling compound in the NaCl-H_2O fluid system.

Based on the results for system fouling for MVC and MVC-FD evaporators, it was found that the MVC-FD system provides a reduction in maximum fouling potential only when the fouling substance precipitates due to liquid volume changes, and when other factors affecting solid solubility either weakly impact solubility or favor precipitation with evaporation. For the MVC-FD it was shown that for a NaCl-$CaSO_4$-H_2O fluid system, the solubility trends prevented solids precipitation across the flash nozzle and instead promoted it across the main heat exchanger. The nozzle did not help to reduce fouling potential in the main heat exchanger, showing that the MVC-FD was ineffective when handling a foulant with solubility trends like that of the NaCl-$CaSO_4$-H_2O fluid system. The MVC-FD evaporator is unlikely to be suitable for seawater desalination if seawater produces the same solubility trends as the NaCl-$CaSO_4$-H_2O fluid system. In cases where temperature increases result in increased solubility of the fouling component, where liquid volume change drives fouling alone, it has been shown that the MVC-FD can remove the fouling potential across the main heat exchanger.

Chapter 5

Conclusions

The MVC and MVC-FD evaporator systems were compared to determine whether the MVC-FD might produce less fouling. The SEC, compression requirements, and main heat exchanger sizing were compared for a variety of operational parameters. Fouling models were developed for MVC and MVC-FD systems processing NaCl-$CaSO_4$-H_2O and NaCl-H_2O fluid systems. These models were used to identify potential applications where MVC-FD evaporation configurations might be better suited than standard MVC systems.

From the steady-state models developed for MVC and MVC-FD evaporator configurations, energy efficiency and performance were determined for multiple evaporator pressure and ΔT_H conditions for both systems. SEC was significantly higher for the MVC-FD configuration relative to the MVC configuration, when compared for varying values of ΔT_H. Depending on the ΔT_H and ΔT_N values for the MVC-FD configuration, the SEC increased by over 100% for the lowest values of ΔT_H and ΔT_N. The percent difference between the SEC of the MVC and MVC-FD systems decreased as ΔT_H values were increased. The MVC-FD had SEC values up to 21.2% greater than the standard MVC configuration with ΔT_H values equal to and greater than 5, with the lowest values of ΔT_N included in the sensitivity studies.

Calculated MVC-FD and MVC main heat exchanger requirements were compared for constant values of ΔT_E. The MVC-FD heat exchanger requirements increase by up to 60% when compared to the standard MVC configuration, even while operating under the lowest ΔT_N values studied. At higher ΔT_E values (greater than 12), the heat exchanger area requirements begin to converge, but these ΔT_E values are well outside operational ranges that yield SEC values for MVC evaporators that are competitive with those of other technologies.

Bulk solubility models developed for NaCl-$CaSO_4$-H_2O and NaCl-H_2O systems were used to compare the maximum fouling potential of MVC and MVC-FD systems. It was shown that the MVC-FD configuration increased potential fouling for the NaCl-$CaSO_4$-H_2O

system, in which $CaSO_4$ acted as the foulant. It was shown that in the NaCl-H_2O system, where NaCl acts as the foulant, scaling potential was significantly reduced. For the NaCl-$CaSO_4$-H_2O system, MVC-FD is an inferior configuration due to its poorer thermal performance and fouling performance. The fouling trends of $CaSO_4$ indicate that solid precipitation is driven mainly by changes in temperature in the MVC-FD system. This differs from the NaCl-H_2O system, where liquid volume change is the main driver for precipitation, which allows precipitation to occur across the flash nozzle. From these results, it was determined that MVC-FD would be useful for conditions in which the formation of scale is driven primarily by liquid volume change, but likely not for systems where precipitation can be caused by increases in temperature.

5.1 Recommendations

As shown in this study, fouling performance is significantly improved using the MVC-FD configuration in comparison to the MVC configuration when fouling is caused by liquid volume change. However, MVC-FD will likely not be used in desalination, due to the results shown by the bulk solubility model for the NaCl-$CaSO_4$-H_2O. However, it should be noted that some benefit might be achieved for this type of system due to the change of heating conditions inside its main heat exchanger caused by preventing boiling. Only a model that incorporates precipitation kinetics, diffusion modelling, and specific equipment design, or experimental data can truly capture the changes in fouling in an MVC-FD configuration.

It is recommended that experimental work be done to compare MVC-FD and MVC evaporator conditions with respect to fouling to more assuredly resolve whether there are potential applications for MVC-FD in desalination. Additionally, work should be done to identify other situations where the MVC-FD configuration would be applicable, according to the results of the NaCl-H_2O solubility model. Ideally this would include experimental confirmation.

References

Alsadaie S., Mujtaba I., 2017. Dynamic modelling of heat exchanger fouling in multistage flash (MSF) desalination. Desalination. 409, 47-65.

Al-Sofi M.A.K., 1999. Fouling phenomena in multi stage flash (MSF) distillers. Desalination. 126, 61-76.

Amy G., Ghaffour N., Li Z., Francis L., Linares R.V., Missimer T., Lattemann S., 2017. Membrane-based seawater desalination: Present and Future Prospects. Desalination. 401 16-21.

Awad M., 2011. Fouling of Heat Transfer Surfaces, Heat Transfer - Theoretical Analysis, Experimental Investigations and Industrial Systems, Belmiloudi A. (Ed.). 505-540.

Aybar H., 2002. Analysis of a mechanical vapour compression desalination system. Desalination. 142, 181-186.

Azimi G., Papangelakis V.G., Dutrizac J.E., 2007. Modelling of calcium sulphate solubility in concentrated multi-component sulphate solutions. Fluid Phase Equilibria. 260, 300-315.

Bahar R., Hawlader M.N.A., Woei L., 2004. Performance evaluation of a mechanical vapour compression desalination system. Desalination. 166, 123-127.

Burn S., Hoang M., Zarzo D., Olewniak F., Campos E., Bolto B., Barron O., 2015. Desalination techniques – A review of the opportunities for desalination in agriculture. Desalination. 364, 2-16.

Darwish M., 1988. Thermal analysis of vapour compression desalination system. Desalination. 69, 275-295.

Esawy M., Malayeri M.R., 2017, Modeling of $CaSO_4$ crystallization fouling of finned tubes during nucleate pool boiling. Desalination, 118, 51-60.

Ettouney H., 2006. Design of single-effect mechanical vapour compression. Desalination. 190, 1-15.

Freyer D., Voigt W., 2000. Crystallization and phase stability of $CaSO_4$ and $CaSO_4$-Based Salts. Monatshefte für Chemie. 134, 693-719.

Fritzmann C., Löwenberg J., Wintgens T., Melin T. 2007., State-of-the-art of reverse osmosis desalination. Desalination, 216, 1-76.

Gammon P., Dinn G., Whitten J, inventors; Inland Technologies Inc, assignee. Method for removing water from an aqueous fluid mixture. US Patent 6120651. September 19, 2000.

Hameeteman E., 2013. Future Water (In) Security: Facts, Figures, and Predictions. Global Water Institute.

Harker J.H., Backhurst J.R., Richardson J.F., 2003. Chemical Engineering. Vol. 2, 5th ed. Butterworth-Heinemann

Holmgren M., 2007. X Steam, Thermodynamic Properties of Water and Steam.

Jamialahmadi M., Müller-Steinhagen H., 2010. Desalination and Water Resources: Physical, Chemical and Biological Aspects of Water - Crystallization fouling.

Kester D.R., Duedall I., Connors D.N., Pytkowitz R.M., 1967. Preparation of Artificial Seawater. Limnology and Oceanography. 12, 176-179.

Khawaji A., Kutubkhanah I., Wie J.M., 2008. Advances in seawater desalination technologies. Desalination. 221, 47-69.

Kind, M., Mersmann, A., 1990. On Supersaturation During Mass Crystallization from Solution. Chemical Engineering Technology. 13, 50−62.

Kishi M., inventor; Aquasystems Inc., assignee. Single stage flash evaporation apparatus based on mechanical vapour compression method. European Patent 1798202B1. July 17, 2013.

Koros W., 2004. Evolving beyond the thermal age of separation processes: Membranes can lead the way. AIChe Journal. 50, 2326-2334.

Krömer K., Will S., Loisel K., Nied S., Detering J., Kempter A., Glade H., 2015. Scale formation and mitigation of mixed salts in horizontal tube falling film evaporators for seawater desalination. Heat transfer engineering. 36, 750-762.

Manjula N., Kumar D., 2013. Water desalination and challenges: The Middle East perspective: a review. Desalination and Water Treatment. 51, 2030-2040.

Marshall W., Slusher R., 1966. Thermodynamics of calcium sulfate dihydrate in aqueous sodium chloride solutions, 0-110°C. Journal of Physical Chemistry. 70, 4015–4027.

Marshall W., Slusher R., Jones E., 1964. Aqueous Systems at High Temperatures XIV. Solubility and Thermodynamic Relationships for $CaSO_4$ in NaCl-H_2O Solutions from 40 to 200 C., 0 to 4 Molal NaCl. Journal of Chemical and Engineering Data. 9, 187–191.

MATLAB. 2018. Natick, Massachussetts: Mathworks.
https://www.mathworks.com/products/matlab.html

MEGlobal, 2008. Ethylene Glycol Product Guide.
http://www.meglobal.biz/media/product_guides/MEGlobal_MEG.pdf

Meijer J.A.M., Van Rosmalen G.M., 1984, Solubilities and supersaturations of calcium sulfate and its hydrates in seawater. Desalination. 51, 255-305.

Mota F.L., Carneiro A.P, Queimada A., Pinho S.P., Macedo E.A., 2009. Temperature and solvent effects in the solubility of some pharmaceutical compounds: Measurements and modeling. European Journal of Pharmaceutical Sciences. 37. 499-507.

Oliveira S.B.M., Marques R.P., Parise J.A.R., 2001. Modelling of an ethanol-water distillation column with vapour recompression. International Journal of Energy Research. 25, 845-858.

Power W., Fabuss B., Satterfield C., 1966. Transient solute concentrations and phase changes of calcium sulfate in aqueous sodium chloride. Journal of Chemical and Engineering Data, 11, 149-154.

Prante J., Ruskowitz J.A., Childress A.E., Achilli A., 2014. RO-PRO desalination: An integrated low-energy approach to seawater desalination. Applied Energy. 120. 104-114.

Rahman F., 2013. Calcium sulfate precipitation studies with scale inhibitors for reverse osmosis desalination. Desalination. 319, 79-84.

Rahman F., Amjad Z., 2009. Scale Formation and Control in Thermal Desalination Systems. The Science and Technology of Industrial Water Treatment. 272-296.

Revelle R., 1934. Physico-chemical factors affecting the solubility of calcium carbonate in sea water. J. of Sedimentary Research. 4, 103-110.

Sandei L., D'Antonio R., Leoni C., Cacace D., Palmieri L., 2003. Application of Mechanical Vapour Compression for Liquid-Food Concentration. Industria Conserve. 78, 451-457.

Seidell A., 1919. Solubilities of inorganic and organic compounds; a compilation of quantitative solubility data from the periodical literature. Van Nostrand, New York.

Sharqawy M., Leinhard J., Zubair S., 2010. Thermophysical properties of seawater: a review of existing correlations and data. Desalination and Water Treatment. 16, 354-380.

Shatat M., Riffat S.B., 2014. Water desalination technologies utilizing conventional and renewable energy sources. International Journal of Low-Carbon Technologies. 9, 1-19.

Singh Y., Shazad M., NG K., 2017, Scale Formation in Thermally-driven Seawater Desalination: Evaluation of Tetrapolymer Antiscalant at Higher Temperature Operation. International Water Technology Conference. 20, 412-423.

Sinnott R.K., 2005. Coulson & Richardson's Chemical Engineering. Vol. 6, 4th ed. Butterworth-Heinemann.

Smith J.M., Van Ness H.C., Abbott M.M., 2005. Introduction to Chemical Engineering Thermodynamics. McGraw-Hill.

Stärk A., Krömer K., Loisel K., Odiot K, Nied S., Glade H., 2017. Impact of Tube Surface Properties on Crystallization Fouling in Falling Film Evaporators for Seawater Desalination. Heat Transfer Engineering. 38, 762-774.

Stillwell A., Webber M., 2016. Predicting the specific energy consumption of reverse osmosis. Water. 8, 601.

Subramani A, Jacangelo J.G., 2015. Emerging desalination technologies for water treatment: A critical review. Water Research, 75, 164-187.

Takada M., J.C. Drake J.C., 1983. Application of improved high performance evaporator, Desalination, 45, 3-12.

Van Driesseche A.E.S., Stawski T.M., Benning L.G., Kellermeier M., 2017. New perspectives on Mineral Nucleation and Growth: from solution precursors to solid materials: Calcium Sulfate precipitation throughout its phase diagram. Springer International Publishing. Switzerland. Chapter 12. 227-256.

Veza J., 1995. Mechanical vapour compression desalination plants-A case study. Desalination. 101.

Wittering K.E., 2015. Multi-component Crystallisation in the Continuous Flow Environment [dissertation]. Bath: University of Bath.

Zhou Y., Shi C., Dong G., 2014. Analysis of a mechanical vapor recompression wastewater distillation system. Desalination. 353, 91-97.